Cerebral Cortex November 2011;21:2620–2638
doi:10.1093/cercor/bhr048
Advance Access publication April 6, 2011

Descending Projections from Extrastriate Visual Cortex Modulate Responses of Cells in Primary Auditory Cortex

Matthew I. Banks[1], Daniel J. Uhlrich[2], Philip H. Smith[2], Bryan M. Krause[3] and Karen A. Manning[2]

[1]Department of Anesthesiology, [2]Department of Neuroscience and [3]Neuroscience Training Program, University of Wisconsin, Madison, WI 53706, USA

Address correspondence to Dr Matthew I. Banks, Department of Anesthesiology, University of Wisconsin, 1300 University Avenue, Room 4605, Madison, WI 53706, USA. Email: mibanks@wisc.edu.

Primary sensory cortical responses are modulated by the presence or expectation of related sensory information in other modalities, but the sources of multimodal information and the cellular locus of this integration are unclear. We investigated the modulation of neural responses in the murine primary auditory cortical area Au1 by extrastriate visual cortex (V2). Projections from V2 to Au1 terminated in a classical descending/modulatory pattern, with highest density in layers 1, 2, 5, and 6. In brain slices, whole-cell recordings revealed long latency responses to stimulation in V2L that could modulate responses to subsequent white matter (WM) stimuli at latencies of 5–20 ms. Calcium responses imaged in Au1 cell populations showed that preceding WM with V2L stimulation modulated WM responses, with both summation and suppression observed. Modulation of WM responses was most evident for near-threshold WM stimuli. These data indicate that corticocortical projections from V2 contribute to multimodal integration in primary auditory cortex.

Keywords: calcium imaging, cortical column, layer 5, neocortex, patch clamping

Introduction

Sensory cortical columns integrate information arising from diverse sources. Current theories of sensory awareness suggest that neocortex is constantly comparing observed sensory information with what is expected based on experience, context, and information from other sensory modalities (Engel et al. 2001; Hawkins and Blakeslee 2005; Bar 2009). In this model, modulation of sensory responses to external "bottom-up" inputs by internal "top-down" processes is a key component of sensory awareness, but how this modulation occurs within the circuitry of neocortex is unclear. We investigated this integration in murine brain slices using electrophysiological recordings and calcium imaging of neural activity in the primary auditory cortical area Au1 in response to white matter (WM) stimuli and modulatory stimuli applied to a descending projection to Au1.

Afferent input terminals within a cortical column are segregated according to their source, allowing information flowing up and down the cortical hierarchy to contact cells and subcellular regions in a lamina-specific manner. In primary sensory cortex, thalamocortical afferents arising from specific thalamic nuclei (lemniscal thalamocortical fibers) terminate with highest density in layer 4 and deep layer 3 (Frost and Caviness 1980; Scheel 1988; Huang and Winer 2000), contacting dendrites of cells with somata in layers 3–6 (Mitani et al. 1985; Hefti and Smith 2000; Cruikshank et al. 2002). Descending afferents and afferents from nonspecific thalamus eschew the granular layer and terminate with highest density in layers 1, 2, 5, and 6 (Ryugo and Killackey 1974; Herkenham 1980; Galaburda and Pandya 1983; Arnault and Roger 1990; Clerici and Coleman 1990; Felleman and Van Essen 1991; Rouiller et al. 1991; Shi and Cassell 1997; Huang and Winer 2000; Linke and Schwegler 2000), forming a termination zone complementary to ascending afferents. Some individual cells, such as large layer 5 pyramidal cells, are positioned to integrate directly afferent input from both sources, while other cells may participate in this integration via local circuits.

Multimodal integration is an important example of coordination between cortical areas as stimuli arising in the natural world typically activate multiple sensory systems either concurrently or in sequence. The influence of visual information on auditory processing has long been recognized. For example, visual cues from a speaker effectively "amplify" speech sounds in noisy backgrounds (Sumby and Pollack 1954), silent lipreading activates auditory cortical areas in humans (Calvert et al. 1997), and conflicting visual information can alter speech perception (McGurk and MacDonald 1976). All these cases are examples of visual sensory input establishing an expectation for subsequent auditory sensory stimulation, an expectation that is likely mediated by descending cross-modal cortical connections. The sites of multisensory integration have attracted renewed interest in the last several years (Ghazanfar and Schroeder 2006; Macaluso 2006; Driver and Noesselt 2008), and accumulating evidence suggests that primary sensory cortex is an important locus (Fu et al. 2003; Ghazanfar et al. 2005; Murray et al. 2005; Lakatos et al. 2007, 2009; Martuzzi et al. 2007; Kayser et al. 2008; Liang et al. 2008). In auditory cortex, it has been shown that somatosensory or visual stimuli can modulate responses to the auditory stimuli, and this modulation can be facilitative or suppressive depending on the individual neuron and the context (Ghazanfar et al. 2005; Bizley et al. 2007; Kayser et al. 2007, 2008; Lakatos et al. 2007). Extrastriate visual cortex (V2) in rodents has been shown to play a key role in coordinating multisensory integration (Hirokawa et al. 2008), and previous reports demonstrate that V2 projects to primary auditory cortex in rats, gerbils, and ferrets (Miller and Vogt 1984; Budinger et al. 2006; Bizley et al. 2007; Smith et al. 2010).

Here, we show that neurons in V2 project to Au1 in mice in a pattern typical of descending cortical projections, with dense labeling in supragranular and infragranular layers. We also provide evidence that these projections are preserved in brain slices, enabling us to test their function using a calcium imaging technique in which fluorescence signals are monitored simultaneously in dozens of individually identified cells. Stimulation of the WM in neocortical brain slices has been

shown previously to activate cells throughout the cortical depth but in a horizontally restricted manner, with the dimensions of this horizontal spread comparable to those of a cortical column (Contreras and Llinas 2001). We show that activation of V2 modulates responses of neurons in Au1 to WM stimuli. This modulation primarily appears as summation but in some cases can be suppressive, suggesting that inputs from V2 can activate both excitatory and inhibitory processes to control columnar information flow in Au1.

Materials and Methods

All experimental protocols conformed to American Physiological Society/National Institutes of Health (NIH) guidelines and were approved by the University of Wisconsin Animal Care and Use Committee.

Anterograde Labeling In Vivo

Male and female mice (postnatal days 60–160) were premedicated for pain and intraoperative swelling with ketoprofen (5 mg/kg), anesthetized with isoflurane (1–1.5% in 100% O_2), and placed in a stereotaxic apparatus (Kopf Instruments). Adequacy of anesthesia was determined by response to toe pinch. Body temperature was maintained with a heating pad (Equine Right Spot). The dorsal surface of the skull was exposed via a midline skin incision and small craniotomies drilled to allow access to underlying extrastriate cortex.

To study visual cortical projections to auditory cortex, biotinylated dextran amine (BDA; molecular weight 10 000; Sigma-Aldrich) injections were made into medial (V2M) and lateral (V2L) extrastriate visual cortex. Higher order extrastriate cortex surrounds primary visual cortex, and the medial and lateral extrastriate regions have long been identified as separate regions (Heumann et al. 1977). Studies suggest the presence of distinct subregions within mouse medial and lateral extrastriate cortex (Caviness 1975; Wagor et al. 1980; Olavarria and Montero 1989; Wang and Burkhalter 2007); however, the number and relative position of these areas within the visual cortical hierarchy remain unclear. The stereotaxic coordinates and the terminology of Franklin and Paxinos (2008) were used. V2L corresponds roughly to regions V3 and V2 described by Wagor et al. (1980) and the rostrolateral, anterolateral, lateral, and posterior regions described by Wang and Burkhalter (2007). V2M is further subdivided by Franklin and Paxinos (2008) into a medial and lateral portion, but these were considered together as V2M for the purposes of this study. V2M corresponds roughly to the posteromedial region described by Wagor et al. (1980) and the ventromedial regions and part of V2 described by Wang and Burkhalter (2007). For V2L injections, a craniotomy was drilled between 2.5 and 4.5 mm caudal to bregma and 3–3.5 mm lateral to the midline. For V2M injections, a craniotomy was drilled between 2.5 and 4.5 mm caudal to bregma and 1.5 mm lateral to the midline. There was considerable variability in the distance between lambda and bregma landmarks in these mice. Successfully placed injections were confirmed histologically.

A glass electrode (outer tip diameter of 20–30 μm) filled with 6% BDA in saline was visually guided to the exposed surface of the cortex and manually advanced 500 μm into the brain. BDA was injected iontophoretically (5–7 μA anodal current: 7 s on, 7 s off) for 10–15 min. The electrode was left in place for an additional 10 min and withdrawn.

Postinjection Processing

The wound was sutured and treated with a broad spectrum antibiotic and lidocaine and the animal monitored daily for signs of discomfort or infection. Ketoprofen (5 mg/kg q12 h intraperitoneally) was administered postoperatively for pain. Five to 7 days after surgery, animals were deeply anesthetized with sodium pentobarbital (90 mg/kg) and perfused intracardially with 100–200 mL of 0.9% phosphate-buffered saline (PBS) followed by 300–500 mL of a 3% paraformaldehyde/1% glutaraldehyde solution in 0.1 M sodium phosphate buffer (pH 7.4).

Brain tissue was processed using methods described previously (Smith et al. 2010). The tissue was refrigerated for 1 h and the brain removed and placed in the same fixative overnight. Coronal sections (70 μm thick) were made using a vibrating microtome, and the tracer was visualized using the diaminobenzidene-nickel/cobalt intensification method (Adams 1981). Sections were rinsed in phosphate buffer and inspected with a light microscope to determine whether the gross injection had successfully labeled axons in auditory cortex. Some of the sections containing terminals were selected to be processed for electron microscopy (EM). Sections not selected for EM were mounted on slides and dehydrated. Half of these sections were stained with cresyl violet and coverslipped, while the other half were coverslipped unstained.

High–molecular weight BDA (10 000) is primarily an anterograde marker that yields fine labeling of abundant numbers of axons and terminals (Reiner et al. 2000). Nevertheless, retrograde labeling in locations distant to the injection site can occur. Following 2 BDA injections in V2L and 2 injections in V2M, all 4 of which were confined to layers 2–6 and did not invade the underlying WM, we observed dozens of retrogradely labeled cells in visual cortex, but only 2 faintly labeled cells in Au1 and no retrogradely labeled cells were observed in the thalamus or brainstem regions. Thus, while we cannot completely rule out the possibility of some retrograde labeling of axons in the data presented, such labeling is unlikely to affect these findings significantly.

Those sections selected for EM analysis were fixed in 0.5% osmium tetroxide, rinsed in buffer, and dehydrated through a series of graded alcohols and propylene oxide. Sections were then placed in unaccelerated Epon–Araldite resin and transferred into a fresh batch of unaccelerated resin overnight. The sections were then embedded and flat mounted between weighted coated slides and allowed to cure. The portion of the embedded section containing the auditory cortex was isolated from the rest of the section and mounted on a beam capsule. A camera lucida drawing of the flat mounted tissue was made noting the locations of the labeled axons/terminals and nearby fiduciary structures. Thin sections of 70–80 nm were then cut and mounted on grids.

GABA Postembedding Immunogold Labeling

An affinity-isolated γ-aminobutyric acid (GABA) antibody conjugated to bovine serum albumin (BSA; Sigma-Aldrich, Catalog No. A2052) was used to evaluate the GABAergic nature of cortical structures. The thin section, mounted on a nickel grid, was carefully immersed in solution A (0.745 g Tris buffer, 0.9 g NaCl, 0.1 mL Triton X in 100 mL dH_2O, pH 7.6) and 5% BSA for 30 min then in solution A and 1% BSA for 5 min then in solution A and 1% BSA containing the GABA antibody at 1:250 dilution at room temperature overnight. The following day the section was rinsed in solution A and 1% BSA twice for 5 min and once for 30 min then rinsed in solution B (0.688 g Tris buffer, 0.9 g NaCl, 0.1 mL Triton X in 100 mL dH_2O, pH 8.2) for 5 more minutes. The section was then immersed in the secondary antibody (goat anti-rabbit immunoglobulin G with attached 15 nm gold particles) diluted 1:25 in solution B (pH 8.2) for 1 h and rinsed twice in solution A and twice in distilled water. After that they were fixed in 8% glutaraldehyde, rinsed in distilled water, and then counterstained with uranyl acetate and lead citrate and rinsed again. Sections were examined using a Philips CM120 electron microscope. For control sections, the primary antibody step was eliminated.

Analysis of Axon Projection and Terminal Distribution, Light Microscopy

Care was taken to ensure that injections did not spread to the underlying WM. In cases in which the injection site was observed to have involved the WM, the experiments were rejected and the data not analyzed further. As an additional check, we observed no cell bodies labeled in the auditory or visual thalamus following any of the included injections. Labeled axons were plotted by means of a camera lucida attachment under dark field or bright field optics on a Leitz Orthoplan microscope. All labeled axon processes in a section of tissue were incorporated. High-power (×313) camera lucida reconstructions were then digitally scanned and final figures prepared using Adobe Photoshop.

Primary auditory cortex is defined anatomically by its distinctive cytoarchitecture as well as its strong input into intermediate layers from the ventral medial geniculate nucleus of the thalamus. Based on previous studies in mouse (Caviness 1975; Wree et al. 1983; Stiebler

et al. 1997; Cruikshank et al. 2001) and its homology to the rat (Zilles and Wree 1985; Roger and Arnault 1989), primary auditory cortex in mouse is characterized histologically by its thickness and the relatively specific differentiation of its cortical layers including a thick and dense granule cell layer, in contrast to adjacent auditory cortical regions. Anatomically defined primary auditory cortex includes the (histologically defined) area Au1 designated by Franklin and Paxinos (2008), whose terminology is used here. Anatomically defined primary auditory cortex corresponds roughly to physiologically defined regions AAF and A1 described by Stiebler et al. (1997), but unfortunately the correspondence between anatomically defined and physiologically defined subregions is unclear (e.g., there is no generally accepted anatomical subregion corresponding to A1). Because our imaging and electrophysiological recording experiments were performed in brain slices, we refer to the targeted region by its anatomical moniker, that is, Au1, which we could actually confirm post hoc, rather than its physiological moniker, that is, A1, which we would have no way of confirming absent prior electrophysiological recordings in vivo.

To evaluate the distribution of labeled terminals, a high-power (×1000) camera lucida drawing of a narrow strip of primary auditory cortex was made from the cortical surface to the WM below layer 6. All en passant and en terminaux swellings on labeled axons in this cortical strip were represented on the drawing. Cortical layer boundaries were then added to the drawings, and the number of terminals in each cortical layer was counted.

Analysis of Axon Terminals and Their Postsynaptic Targets, EM

For analyzing BDA-labeled axon terminals in auditory cortex arising from V2L, the following procedure was established. A given thin section was manually scanned at ×10 000. After identifying a labeled synaptic terminal, based on the presence of vesicles presynaptically and a postsynaptic thickening of the membrane apposed to the terminal, a photo of the terminal was taken at ×29 000 and its exact location noted on a ×200 camera lucida drawing that had been made of the block face prior to sectioning. Using the ×29 000 image, measurements of the labeled terminal and its postsynaptic target were made for each synapse using The NIH Image/J 1.60 software. Other terminal features were also noted.

In GABA immunogold–labeled material, the "background" gold particle density was calculated for each thin section to account for possible processing differences between sections. Axon terminals or their postsynaptic targets were considered GABAergic if their particle density exceeded the mean gold particle density of the background by 5 times. Background density was measured over non-GABAergic structures such as blood vessel lumens, glial cells, etc.

Retrograde Labeling In Vivo

To determine the boundaries of auditory cortex in brain slice experiments, in some animals layer 5 cells in auditory cortex projecting to inferior colliculus (IC) were retrogradely labeled by injecting fluorescent microspheres into IC (Katz et al. 1984; Christophe et al. 2005). Injections into IC were large and invaded all subdivisions of the central nucleus as well as the external cortex, which should label layer 5 pyramidal cells throughout auditory cortex (Herbert et al. 1991; Doucet et al. 2003). Surgical techniques were identical to those described above for BDA injections, except the craniotomy was located immediately posterior to lambda 1.25 mm off the midline. A glass electrode (outer tip diameter of 20–30 μm) was loaded with ~1 μL red fluorescent beads (Lumaflor) suspended in distilled water. The electrode was visually guided to the exposed surface of the IC and manually advanced 500 μm into the brain. The beads were injected via pressure injection (Picospriter, 10–20 psi, 5–20 ms, 10–20 pulses over 1–2 min). The electrode was left in place for an additional 5 min and withdrawn. The wound was sutured and animals recovered as for BDA injections above. Tissue was harvested for brain slice experiments >48 h after gross injections.

Brain Slice Preparation

Male and female CBA/J mice (postnatal days 21–48) were decapitated under isoflurane anesthesia, and the brains were extracted and immersed in artificial cerebrospinal fluid (ACSF; composed of [in mM] 126 NaCl, 26 $NaHCO_3$, 1.8 KCl, 2.1 $CaCl_2$, 1.4 $MgSO_4$, 1.2 KH_2PO_4, and 10 glucose) at 0–4 °C. Slices (450 μm) were obtained from both hemispheres using standard techniques. We observed that the most consistent responses to V2L stimulation were observed in slices cut ~15 degrees off the coronal plane, with the dorsal edge of the slice caudal to the ventral edge. Slices were maintained in ACSF saturated with 95% O_2/5% CO_2 at 24 °C for >1 h before transfer to the recording chamber, which was perfused at 3 mL/min with ACSF at 34 °C. Au1 and V2L were identified based on their position relative to the rhinal sulcus, midline, and hippocampus, as in previous studies (Metherate and Cruikshank 1999; Cruikshank et al. 2002; Paxinos and Franklin 2003; Verbny et al. 2006), and these locations were confirmed post hoc by fixing slices, staining with cresyl violet, and examining via light microscopy. In some experiments, identifying the boundary between V2L and auditory cortex was aided by prelabeling layer 5 pyramidal cells in auditory cortex with fluorescent latex microspheres injected into IC as described above (Christophe et al. 2005). Labeling was restricted to a band of cells in layer 5 that ran dorsoventrally for a distance of approximately 1–2 mm, consistent with known projections of layer 5 cells of auditory cortex to IC (Herbert et al. 1991; Doucet et al. 2003) and the published location of auditory cortex (Paxinos and Franklin 2003). In these slices, the location of V2L was inferred by the abrupt cessation of labeled cells at the border of auditory and visual cortical areas. Cortical layers were identified by depth relative to the pial surface (Cruikshank et al. 2002; Verbny et al. 2006). We further used the tissue appearance under bright field illumination to identify the approximate borders between cortical layers. Layers 4 and 5B had a relatively dark appearance compared with the light colored bands of layers 3, 5A, and 6.

Anterograde Labeling In Vitro

Biocytin (1% in ACSF) was loaded into a glass pipette (1.7 mm outer diameter, tip diameter 5–10 μm) and applied to layers 3 and 5 in V2L via pressure injection (5–10 psi, 0.1 s, 3 pulses). The boundaries of V2L were determined from a published stereotaxic atlas (Franklin and Paxinos 2008). Following injections, slices were held at room temperature in ACSF bubbled with 95% O_2/5% CO_2 for 4 h, then fixed overnight in 4% paraformaldehyde. Slices were then processed for biocytin staining. Fixed slices were washed in 0.01 M PBS, then incubated in 0.5% H_2O_2 in PBS, then rinsed again for 30 min in 0.01 M PBS. Slices were then incubated overnight in the secondary antibody to the avidin–biotin–horseradish peroxidase (HRP) complex (ABC Kit, Vector Labs) in PBS with 0.3% Triton X-100 and 2% BSA. On the second day, the slices were rinsed in 0.1 M PBS, and the HRP was reacted using 0.04% diaminobenzidine with dimethyl sulfoxide (DMSO) and nickel/cobalt intensification. A 0.01% H_2O_2 in 0.1 M PBS was then added for 15 min, then the slices were rinsed for 40 min in PBS and mounted on slides and allowed to air-dry. The mounted sections were then stained with cresyl violet and coverslipped.

Extracellular Electrophysiological Recordings

Extracellular field potentials were recorded using patch pipettes fabricated from borosilicate glass (KG-33; 1.7 mm outer diameter; 1.1 mm inner diameter; Garner Glass) using a Flaming–Brown 2-stage puller (P-87; Sutter Instruments). The tips of the pipettes were broken under visual control to an outer tip diameter of 10–15 μm and had open-tip resistances of 0.5 MΩ when filled with ACSF. Data were amplified (MultiClamp-700A; Molecular Devices), low-pass filtered (10 kHz), digitized (20 kHz; DigiData 1322A; Molecular Devices), and recorded using pClamp version 9.2 (Molecular Devices).

Patch-Clamp Electrophysiology

Cells were visualized using a video camera (Oly110; Olympus) connected to the upright microscope (Olympus BX60-WI) with a long working-distance water-immersion objective (Olympus ×40, 0.9 numerical aperture (N.A.)) and differential interference contrast optics. In some experiments, we chose cells that responded to stimulation in WM or V2L with [Ca] transients. In these cases, the cell was identified

under fluorescence microscopy and then localized for patch-clamp recording using simultaneous light and fluorescence microscopy before switching to differential interference contrast (DIC). In other experiments, cells were selected based on their location and healthy appearance under DIC optics. Patch pipettes were fabricated from borosilicate glass as for extracellular recordings. Tip shape and diameter were adjusted to give open-tip resistances of 2–4 MΩ so that access resistances of <20 MΩ may be readily achieved. Pipettes were filled with (mM) KGluc 140, NaCl 10, ethyleneglycol-bis(2-aminoethylether)-N,N,N′,N′-tetra acetic acid 0.1, MgATP 2, 4-(2-hydroxyethyl)-1-piperazineethanesulfonic acid 10, pH 7.2. Pipettes were mounted and positioned using an integrated, motorized 4-dimensional translation system (Siskiyou Inc.). Tight-seal whole-cell recordings were obtained as described previously (Merriam et al. 2005). Electrophysiological signals were recorded as for extracellular data above.

Fiber Stimulation

Afferents were activated using pairs of tungsten electrodes (0.1 MΩ, 75 μm diameter; FHC Inc.) cemented together at tip separations of ~50–200 μm with dental acrylic and wax. Stimuli were applied to the WM just deep to the imaged area in auditory cortex. In extracellular recordings of local field potentials (LFPs; not shown), these stimuli activated a vertical strip of tissue from layer 6 to layer 1 and this activation was restricted to ~250 μm on either side of the electrode in the lateral (i.e., horizontal dimension), similar to previous reports (Contreras and Llinas 2001). A second set of stimulating electrodes was placed in V2L in layer 5. Stimuli (100 μs, 10–250 μA) were applied using constant current stimulus isolation units (A365, WPI Inc.) and consisted of either single pulses or brief trains (2–20 pulses, 40 Hz).

Ca Imaging: Cell Loading

Cells were loaded with the membrane-permeant form of the calcium-indicator dye Oregon Green BAPTA-1 (OGB-1 acetoxymethyl (AM) ester form; Invitrogen) using the multicell bolus loading technique (Stosiek et al. 2003; Kerr et al. 2005). In this technique, pressure injection of the dye at high concentration into the tissue preferentially labels neurons (vs. glial cells) in a spherical area ~100–200 μm in diameter. Intracellular fluorescence rises to a stable level within an hour and remains stable for > 4 h after reaching this plateau. Multiple sequential injections in the slice allowed for a series of imaging experiments to be performed in the same slice over a 10-h period. Imaging data presented here represent responses of cells in layers 3–6; however, the majority of cells were imaged in layer 5. Specific loading details are as follows. OGB-1 AM was dissolved in DMSO containing 20% pluronic acid to a dye concentration of 5 mM. Loading pipettes were fabricated from borosilicate glass (KG-33; 1.7 mm outer diameter, 1.1 mm inner diameter; Garner Glass) using a Flaming–Brown 2-stage puller (P-87; Sutter Instruments). Pipettes had outer tip diameters of ~2 μm and were filled with <1 μL of the dye solution. The solution was applied to the tissue using pressure injection (Picospitzer II; General Valve; 5–10 psi, 1–10 s pulses over 1–2 min) at a depth of 50 μm. After injection, the location of the injection site was recorded using captured still images and the pipette retracted from the tissue. Four or 5 injections were typically made over a period of 30–60 min. An additional 30–60 min were allowed for background dye to be washed away and intracellular fluorescence to stabilize.

Ca Imaging: Data Collection

A spinning disk confocal microscope (Olympus BX-61 DSU) with excitation filter 480–510 nm and emission filter 495–595 nm (Chroma U-N41026/C67083) and a ×40 (Olympus LUMPlanFL/IR, N.A. = 0.8, field of view diameter = 200 μm), ×20 (Olympus UMPlanFL, N.A. = 0.5, field of view diameter = 400 μm), or ×10 (Olympus UMPlanFL, N.A. = 0.3, field of view diameter = 800 μm) water-immersion objective was used for imaging experiments. Images were captured at 10–50 frames/s with a cooled CCD camera (Hamamatsu C9100) using SimplePCI software (v6.1; Hamamatsu Corp.). Typically, data were collected for 20–60 s in a 3-condition sequence in which stimuli were applied to the WM, then to V2L, and then to V2L and WM in combination, with 5–10 s between stimuli.

Ca Imaging: Data Analysis

Individual cells were localized within the cortical layers by comparison to bright field still images and their activity measured as change in relative fluorescence (%ΔF/F) over time. Using this technique, we could identify typically 70–100 cells at ×40 in an imaged field. Cells from this population were targeted for further analysis by computing a response map for each stimulus event—the difference between the average image florescence during the 2 s following the stimulus and the average image florescence 2 s before the stimulus. Areas of increased florescence identified in this way almost always corresponded to labeled cells identified in the average images from the full movie. This initial preselection process was liberal; any cell in which a response was detected (see below) to even a single stimulus event was selected for further analysis. More stringent quantitative criteria described below were applied to identify responsive cells, which comprised roughly one-third of the preselected sample.

Fluorescence signals from identified cells were analyzed using custom software written in Matlab (Mathworks). Responses to afferent stimulation were detected as follows. A peak detection algorithm calculated the difference in amplitude of the fluorescence signal between 2 windows separated by a user-defined time period (typically 1 s) and compared this difference with the standard deviation (SD) of the difference signal calculated over the previous 2 s. The algorithm detected a peak when the difference signal exceeded its SD by a factor of 2-fold for at least 0.2 s. If no peak was detected within a response window of 2 s following afferent stimulation, the magnitude of the fluorescence signal corresponding to this "failure" was calculated as the mean fluorescence signal within that response window.

To determine whether stimulation in V2L modulates the responses of cells to WM stimulation, we compared quantitatively the responses to paired stimulation (R_{Pr}) versus WM alone (R_{WM}). Because we typically recorded only 3 or 4 responses to each stimulus in a given cell, using paired *t*-tests corrected for multiple comparisons for >1400 cells leads to an overly conservative estimate for the number of significantly affected cells. Instead, we employ a local false discovery rate method originally described by Efron (2004) that is particularly well suited to large-scale multiple hypothesis testing. We computed the ratio of the paired response to the WM response for each cell (R_{Pr}/R_{WM}), yielding an estimate of this data distribution based on our population of 1417 cells. The null hypothesis for each cell is that this ratio would be unity, that is, there is no difference between R_{Pr} and R_{WM}. Any deviation from unity is due to 2 sources of variability: 1) trial-by-trial variability in the WM response and 2) a significant effect of the preceding V2L stimulus on the WM response. We wish to separate these 2 sources of variability so that we can estimate the proportion of cells whose WM responses are significantly affected by V2L stimulation. Our assumption is that ratios close to unity are not significant, while those far from unity are significant; the question is where to draw the line. The local false discovery rate method takes the ratio of the observed data distribution, which is a mixture of the significant data points and an underlying null distribution (the latter representing the WM trial-by-trial variability), to an estimate of the null distribution. Those responses whose frequency of observation is far more common in the data distribution than in the null distribution are considered significant.

We compared the number of cases in each bin of the data distribution with the number of cases in that bin of the null distribution. Bins for which the number of observed data cases was more than 5 times that expected from the null distribution were considered to be significant; cells whose magnitude of R_{Pr}/R_{WM} lie within that bin were flagged in the plots of Figure 13*B,C*. The critical value of the ratio, here chosen to be 0.2, is an upper bound on the percentage of cells identified as significant that are in fact not (false positives). This misidentification arises due to the overlap of the 2 distributions; for example, in Figure 13*A*, the first significant bin to the left of unity has a number of null observations as well, which would be falsely identified as significant. This can also work the other way; for example, in the next bin closer to unity, there are likely a number of significant cells that did not fall within the criterion for significance. (Note that this criterion does not imply that 20% of the entire data set would be expected to be falsely identified as significant.)

To estimate the null distribution, we used the responses to WM stimulation alone as follows. For each cell with N_{Trial} WM responses (or failures), we took all combinations of $N_{Trial}/2$ responses and computed all permutations of the ratio of the means of these subsets. For example, if there were 4 responses, R_1, R_2, R_3, R_4, we computed mean(R_1, R_2)/mean(R_3, R_4), mean(R_1, R_3)/mean(R_2, R_4), etc. The null distribution was composed of all these ratio values. For the null distribution, we only included cells for which there were at least 4 WM responses and in which there was a detected WM response (i.e. non-failure) on at least one trial (327 of 1417 cells). The estimated null distribution matched closely the central portion (i.e., the portion centered on unity ratio) of the observed data distribution (see Results and Fig. 13*A*), consistent with our intuition that those cells with ratios close to unity are not significantly affected by V2L stimulation, while those cells in the tails are significantly affected.

Responses to paired WM and V2L stimulation (R_{Paired}) were compared with responses to WM stimulus alone (R_{WM}) by computing the difference R_{Paired} – R_{WM}. Values <0 indicated suppression of the response to WM by V2L stimulation, while values >0 indicated summation of responses to V2L and WM stimulation.

Solutions and Drugs

All reagents not specified above were obtained from Sigma-Aldrich.

Digital Processing of Images

Digitized light-level photomicrographs were acquired with a Spot camera (Diagnostic Instruments) mounted on a Nikon Eclipse E600 microscope using a ×40 oil objective, dark field illumination or bright field illumination with Nomarski optics. The final figures were prepared using Adobe Photoshop, and tonal adjustments were applied across the entire image (curves, contrast, and unsharp mask functions) with no further manipulations.

Results

Projections from V2 to Au1 in Mouse—In Vivo and In Vitro Anterograde Labeling

Previous studies have suggested that in rats, extrastriate visual cortex sends a projection to primary auditory cortex (Miller and Vogt 1984; Smith et al. 2010). We confirmed that an equivalent projection is observed in mice using anterograde labeling studies in vivo and in vitro.

We made injections of BDA into extrastriate visual cortical areas both medial (V2M; n = 2) and lateral (V2L; n = 2) to primary visual cortex in vivo (Fig. 1). As previously described in rat (Miller and Vogt 1984), labeled visual cortical axons were found in Au1 primarily in superficial and deep layers (Fig. 1*A*,*B*). Closer inspection of these axons (Fig. 1*C*–*F*) revealed both en passant (Fig. 1*D*,*F*, arrowheads) and en terminaux (Fig. 1*E*, asterisk) swellings. Labeled swellings observed with the electron microscope (Fig. 1*G*,*H*) form synapses on small dendrites and dendritic spines. In a small population (n = 9) of these swellings inspected at the electron microscopic level in tissue labeled with a GABA antibody (not shown), most (8/9) were presynaptic to GABA immunonegative structures, suggesting that the projection from V2 terminates primarily on non-GABAergic dendrites, consistent with our previous findings (Smith et al. 2010).

A more quantitative evaluation of these terminals is seen in Figures 2 and 3. Figure 2*A* shows an injection site localized to V2M (asterisk). The distribution of axonal swellings across layers in a strip of primary auditory cortex (Fig. 2*C*, brackets) resulting from this injection is shown in Figure 2*B*. The majority of terminals are concentrated in layers 1 (29.6% of total terminals) and 6 (43.4%) with the fewest in layers 4 (3.6%) and 2/3 (8.0%). The layer 1 terminals are concentrated in the superficial half of the layer. Figure 2*C* illustrates that the visual cortical innervation extends for a considerable distance rostrocaudally and that the inputs extend into other cortical areas as well.

A similar injection confined to V2L (Fig. 3*A*, asterisk) also labels corticocortical inputs to Au1. The distribution of labeled corticocortical axons (Fig. 3*C*) extends across the auditory cortical laminas rostrocaudally but largely avoids layer 4. The terminal distribution of this projection is similar in some ways to the V2M input with the majority of terminals concentrated in layers 1 (29.7%) and 6 (29.7%) and the fewest in layer 4 (2.6%). However, unlike the projection from V2M, terminals originating in V2L are distributed throughout layer 1 and in addition provide a moderately strong innervation of layers 2 and 5. Thus, medial and lateral extrastriate visual cortical inputs to primary auditory cortex are in the form of a feedback connection (Felleman and Van Essen 1991) with terminals ending primarily in superficial and deep layers. Following injections into V2, numerous retrogradely labeled cells were observed in V1 and in the other V2 area (e.g., in V2M for a V2L injection), but we almost never observed retrogradely labeled cells in Au1 (2 cells in 1 injection and none in 3 other injections). Thus, the connection from V2 to Au1 does not appear to be reciprocal. The 2 retrogradely labeled cells in Au1 were labeled lightly with no evidence of labeled axon collaterals in Au1. Thus, the terminal distributions in auditory cortex reflect the projection from V2 without contamination by terminals originating in retrogradely labeled cells.

These experiments indicated that visual cortical cells and their auditory cortical projections and terminations could be located at nearly the same rostrocaudal level, suggesting that a coronal brain slice should contain intact connections from visual to auditory cortex. In practice, we found that a section 15 degrees off of coronal, with the dorsal surface of the slice at a more caudal level, preserved the connections from V2L to Au1 most consistently. To verify this, we made biocytin injections into V2L in these off-coronal brain slices containing Au1 (Fig. 4). Gross injections into V2L (Fig. 4*A*,*B*) labeled cell bodies and axons that projected to Au1 (Fig. 4*C*). Also note that in 5 slices in which gross injections into V2L were performed, only one retrogradely labeled cell in Au1 was observed, consistent with the results of gross injections in vivo presented above, though numerous such cells were observed in V1 and V2M. Thus, as in other species where at best a weak reciprocal projection from Au1 to V2L has been reported (Miller and Vogt 1984; Falchier et al. 2002; Rockland and Ojima 2003; Budinger et al. 2006; Bizley et al. 2007; Hall and Lomber 2008; Meredith et al. 2009), this connection is likely to be minor in the mouse.

Monitoring Activity in Au1 Using Calcium Imaging

We have presented anatomical evidence for a descending cortical projection from V2 to Au1. We next used calcium imaging and electrophysiological techniques to determine the functional effect of this projection on cells in Au1 by monitoring responses to stimuli applied to the WM alone or in combination with stimulation in V2L. Data from electrophysiological recordings will be presented below.

Neurons in layers 3–6 of Au1 were labeled with the membrane-permeable form of the calcium dye OGB-1 using pressure

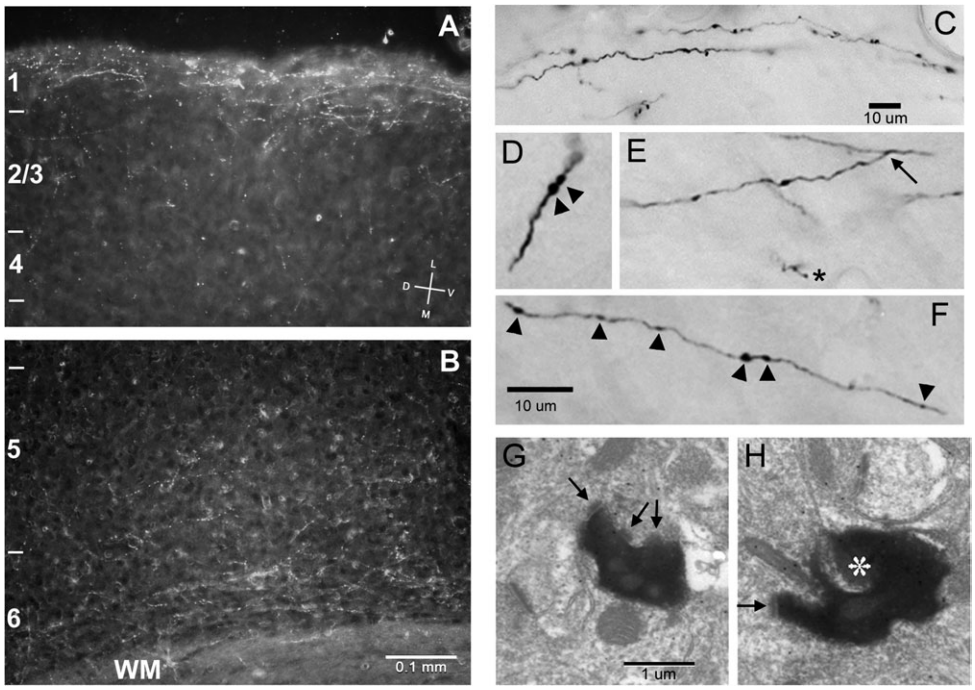

Figure 1. Extrastriate visual cortical axons project to Au1 in mouse. BDA was injected into V2M in vivo. (*A*, *B*) Low-magnification dark field photomicrographs of coronal sections show label (white) predominantly in superficial and deep layers of Au1. Cortical tissue margin is visible near the top of (*A*), running roughly parallel with the figure edge. Cortical layers 1–6 indicated on left. Orientation vane in (*A*) applies to panels (*B*) and (*C*) as well. Scale bar in (*B*) applies to both (*A*) and (*B*). (*C*–*F*) Higher magnification bright field photomicrographs of darkly labeled axons in Au1 layers 1 (*C*) and 6 (*D*–*F*). Arrowheads in (*D*) and (*F*) indicate en passant swellings. Asterisk in (*E*) indicates en terminaux swelling and arrow indicates axonal branch point. Calibration bar for (*D*–*F*) in (*F*). (*G*,*H*) Electron photomicrographs of labeled visual cortical terminal swellings in layers 1 and 2 in Au1. Arrows indicate synaptic specializations. Asterisk in (*H*) indicates dendritic spine. Scale bar in (*G*) applies to (*G*) and (*H*).

injection (Fig. 5*A*). Typically, dozens of cells were labeled sufficiently to identify their somata in fluorescent images (Fig. 5*B*), and fluorescence as a function of time in each cell was monitored (Fig. 5*C*). Stimulation of WM and/or V2L triggered fluorescence increases in a subset of labeled cells as well as a background response. These somatic Ca responses to afferent stimulation were detected using an automated peak detection algorithm (see Methods); we show below that these responses are due primarily to synaptically driven action potential firing in neurons. The background response is likely due to activation of the neuropil (axons, axon terminals, dendrites; Kerr et al. 2005) and was subtracted from fluorescence traces recorded from identified somata. These imaging data are taken from ~3600 labeled cells in 46 slices, of which 1417 exhibited detected responses to afferent stimulation.

The standard stimulation protocol was to apply a train of 4 afferent stimuli at 40 Hz, though the number of pulses in a train was also varied over a wide range. The number of labeled cells in a given area that exhibited Ca responses to afferent stimulation varied with stimulation intensity but was smaller in response to stimulation in V2L (WM: median 12%, first and third quartiles 7.8% and 18%, respectively; V2L: median 4.4%, first and third quartiles 2.2% and 8.7%, respectively; $P < 0.001$, Student's paired *t*-test). Responses to afferent stimulation could be distinguished from 2 types of spontaneous events: 1) events with rapid rise times and moderate decay times that resembled afferent evoked responses and 2) events that had slow rise times (>1 s) and decay times (>3 s) and were assumed to represent activity in labeled glial cells. The latter type of spontaneous activity was extremely rare, with <10 cells exhibiting these events out of >1000 observed. The former type of spontaneous activity was more common but did not interfere with detecting evoked responses. We measured the fluorescence time course in 56 cells from 4 experiments selected at random. In these cells, fluorescence responses had decay time constants of 0.75 ± 0.25 s.

Fluorescence responses typically corresponded to changes of 0.75–5.0%—relative to baseline (ΔF/F; 95% of responses were <5.0%). Although WM stimuli were more likely to activate cells, as described above, response amplitudes were similar for cells responding to WM stimulation (2.2 ± 1.7%, $n = 797$ cells) compared with V2L stimulation (2.5 ± 2.0%; $n = 282$ cells; mean ± SD), though larger stimulation currents were used for V2L (typically 2- to 3-fold difference in intensity). Ca responses were graded with the intensity of afferent stimulation. Increasing either the number of pulses in a stimulus train (Figs 5*C* and 6*A*) or the intensity of the stimulus current with the number of pulses held constant (Fig. 6*B*) triggered Ca responses of increasing amplitudes. Next, we tested the relationship between the number of spikes and the Ca response amplitude.

Ca Responses Represent Synaptically-Driven Action Potential Activity

Before evaluating the interaction between descending and WM stimuli in Au1, we investigated the cellular basis for Ca responses in brain slices. We first show that the electrophysiological correlate of recorded fluorescence transients was action potential firing in labeled cells and that subthreshold synaptic responses do not generate detectable fluorescence signals on single trials. We next show that these spikes were

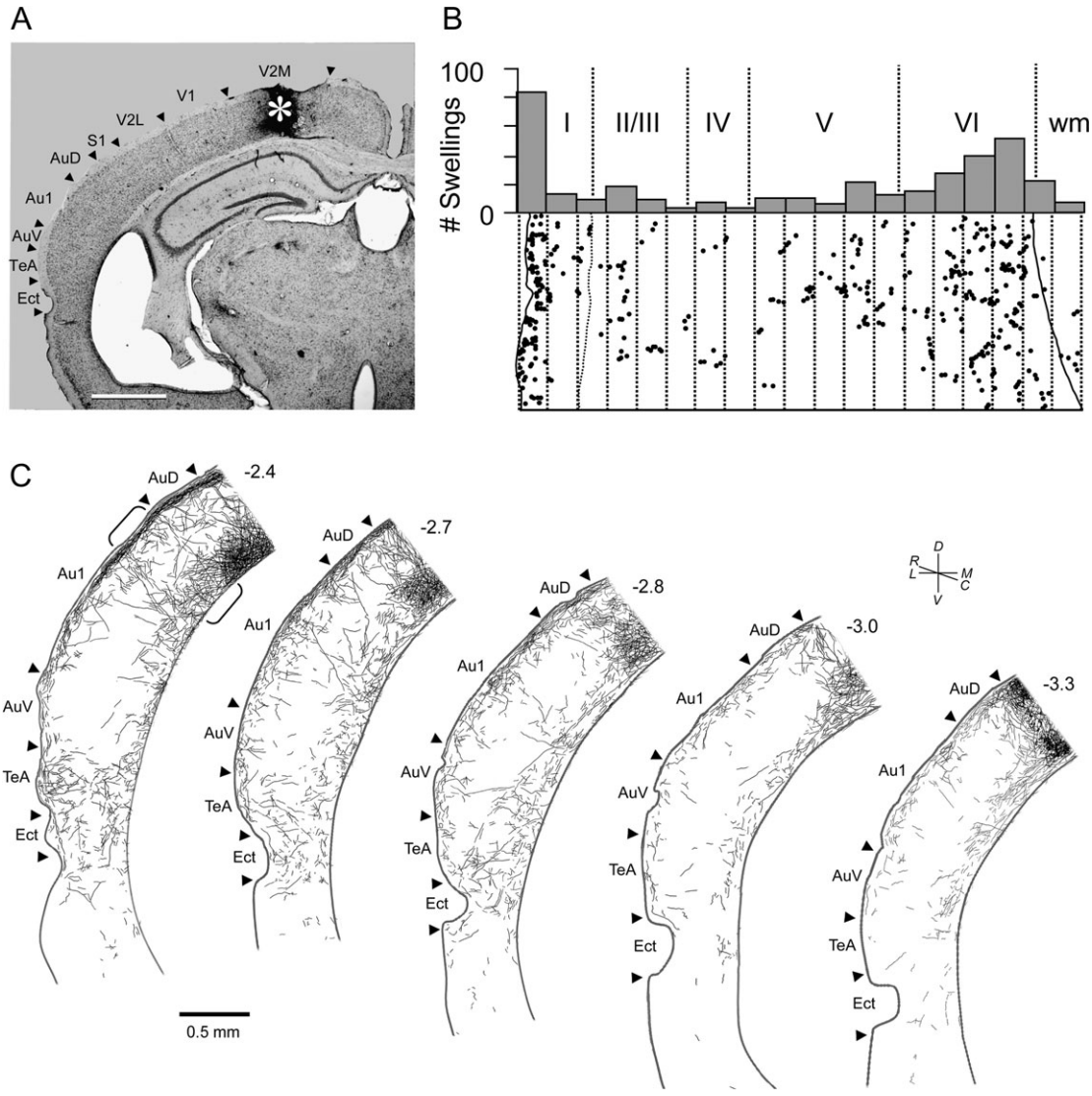

Figure 2. BDA injection into V2M produced anterograde labeling throughout mouse auditory cortex. (*A*) Low-power photomicrograph of a coronal brain section showing the injection site (asterisk). Dorsal is toward the top, lateral is to the left. Scale bar = 1 mm. (*B*) Bottom: Camera lucida drawing of terminal swellings in Au1. Dots indicate the number of terminals in each 50 μm subdivision (dotted lines) from the surface (left) to the WM (right). Top: Plot of the number of terminals in each 50 μm subdivision. Dotted lines demarcate the boundaries of the cortical layers (roman numerals) and the WM. Note high density of labeling in superficial and deep layers. Data were derived from a vertical strip of tissue whose location is indicated by the brackets in (*C*), though the actual tissue used was in section adjacent to the one shown. (*C*) Distribution of labeled axons in camera lucida–reconstructed coronal sections. Level from bregma indicated above each section. Au1, primary auditory cortex; AuD, secondary auditory cortex, dorsal area; AuV, auditory cortex, ventral area; TeA, temporal association cortex; Ect, ectorhinal cortex.

primarily synaptically mediated, as opposed to being due to antidromic or direct activation by electrical stimuli.

To determine the electrophysiological correlates of observed Ca transients, individual cells labeled with OGB-1 and exhibiting Ca responses to WM and/or V2L stimulation were targeted for simultaneous Ca imaging and patch-clamp recording. Because dye fluorescence is rapidly lost upon membrane rupture during whole-cell recordings, we used cell-attached patch recordings to monitor action potential activity in the labeled cell while measuring that cell's fluorescence signal (Fig. 7). In this experiment, the intensity and the number of pulses in a train were varied to elicit between 0 and 5 evoked spikes. In Figure 7*A*, "gray traces" are neuropil Ca responses, "dark traces" are cell Ca responses, and "insets" are on-cell patch recordings from the cell. Stimuli that were subthreshold for triggering spikes generated no detectable Ca response (Fig. 7*A*, bottom), though a background neuropil response was still observed (Fig. 7*A*). A detectable Ca response was observed in this cell for a single spike (Fig. 7*A*, second from bottom). As the number of evoked spikes increased with stimulation intensity or number of pulses, increasing Ca responses were observed. Summary data from recordings such as these in 14 cells show that on average no detectable Ca response is observed in the absence of action potential firing, and response magnitude monotonically increases with the number of spikes (Fig. 7*B*). In this figure, we also plot the mean (0.17%) and mean + 2SD (0.78%) of a sham response calculation, in which the peak detection algorithm was run on data segments in which no stimulation was provided. Note that the mean response to 1 spike (0.83%) falls just outside this sham range. Based on these data, cells were deemed "responsive" to stimulation only if their response

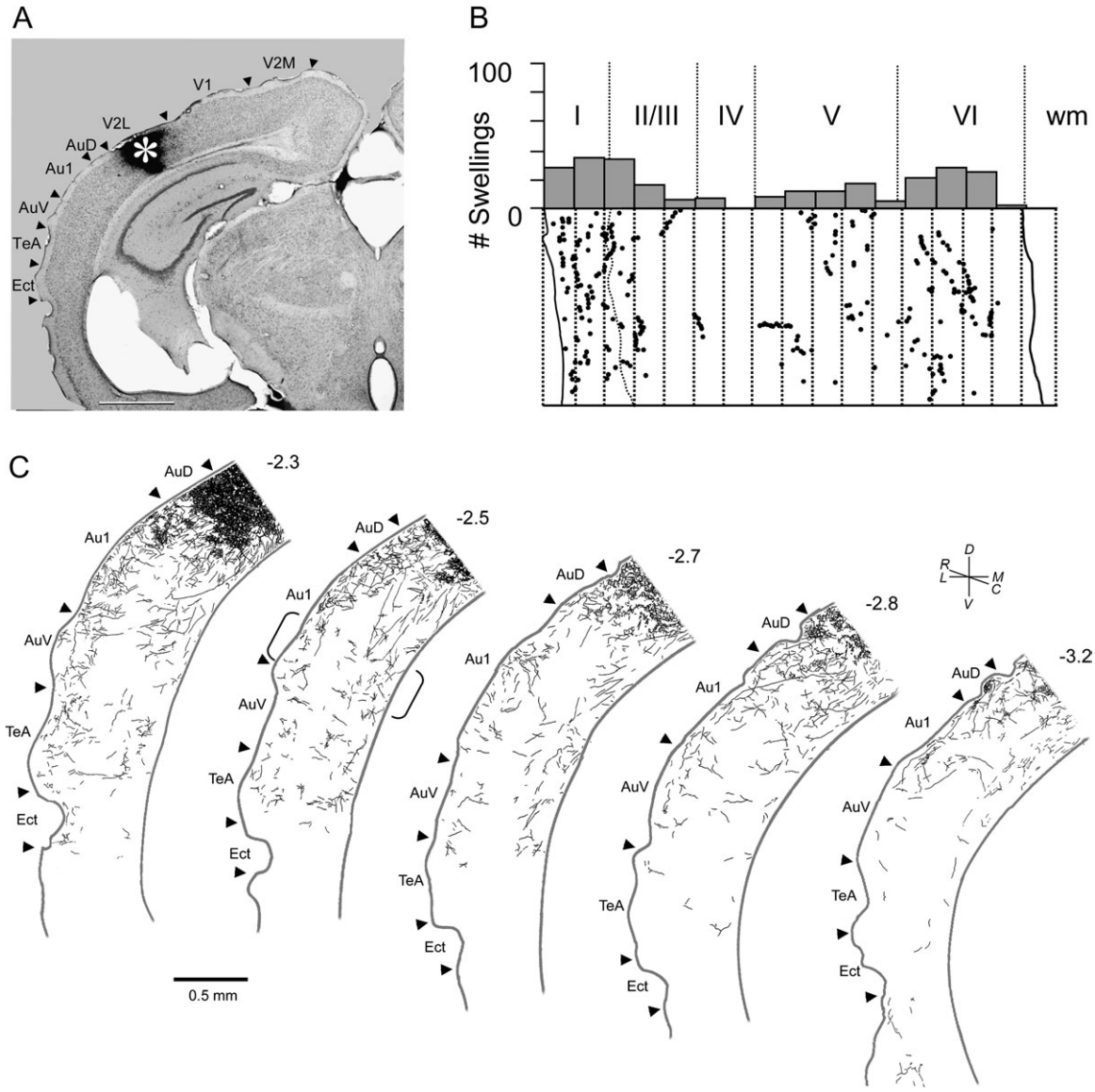

Figure 3. BDA injection into V2L produced anterograde labeling throughout mouse auditory cortex. (*A*) Low-power bright field photomicrograph of a coronal section showing the injection site (asterisk). Dorsal is toward the top, lateral is to the left. Scale bar = 1 mm. (*B*) Camera lucida drawing of terminal swellings in Au1. Note high density of labeling in superficial and deep layers. Data were derived from a vertical strip of tissue whose location is indicated by the brackets in (*C*), though the actual tissue used was in section adjacent to the one shown. (*C*) Distribution of labeled axons in camera lucida–reconstructed coronal sections. Abbreviations as in Figure 2.

amplitudes were >0.78%; this criterion is used explicitly in Figures 8 and 13 below.

In addition, in the cells recorded we did not observe more than one spike fired in response to a single WM or V2L pulse, even at the highest intensities tested (225 μA, up to 4× threshold current). Thus, we expect, in our data, that the number of spikes fired, and thus the Ca response, will be bounded by the number of pulses in a train of stimuli, as long as stimulation intensity is kept within this limit. Based on this observation, we can revisit the data of Figure 6: the increased response amplitude with stimulus intensity and/or pulse number is likely due to increasing numbers of spikes fired per cell during the stimulus train—in the case of increasing intensity, the increased number of spikes being due to fewer and fewer failures during the stimulus train. For example, in Figure 6*B*, one experiment exhibits saturation when the stimulus intensity is increased to 200 μA (filled triangles, solid line) presumably because the cells were already firing on every stimulus pulse in the train at the lower intensity of 125 μA. Very large numbers of pulses could also lead to partial saturation of responses. This is evident between 10 and 20 pulses in Figure 6*A* and is likely indicative of a saturating Ca response, due to either the intrinsic Ca dynamics in the cell or a limitation of the dye. For this reason, nearly all experiments in which we investigated the interaction of V2L and WM stimuli in Au1 were performed using 4 pulses or fewer in stimulus trains.

We have shown that afferent stimulation triggers somatic calcium transients that are due to action potential firing in labeled cells. These spikes are most likely due to super-threshold excitatory synaptic responses but alternatively could be due to either antidromic activation of the axons of labeled cells (e.g., in the case of WM stimulation, these could be layer 5 cells that project via the WM to contralateral cortex and subcortically) or direct activation of labeled cells (e.g., by

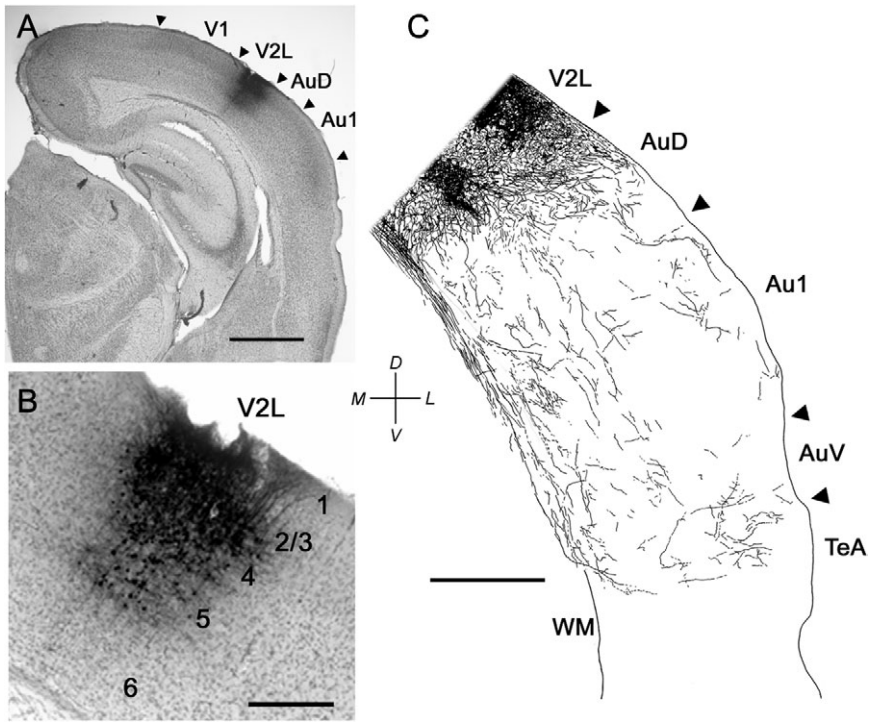

Figure 4. Biocytin injection into V2L in mouse brain slice produced anterograde labeling throughout auditory cortex. (*A*) Low-power bright field photomicrograph showing the injection site in V2L. Scale bar = 1 mm. (*B*) Higher power view of a section adjacent to (*A*) shows labeled cell bodies. Scale bar = 200 μm. (*C*) Labeled axons in camera lucida–reconstructed brain slice following injection in (*A*). Slices are in the off-coronal plane used in physiological and imaging experiments. Orientation vane applies to (*A–C*). Scale bar = 500 μm. Abbreviations as in Figure 2.

activation of voltage-gated channels in the basal dendrites of labeled cells). We used glutamate receptor antagonists to distinguish between these possibilities. We labeled cells in layer 5 or 6 of Au1 and stimulated either in WM (n = 8 slices) or in V2L (n = 7 slices) to evoked Ca responses under control conditions and in the presence of either kynurenic acid (4 mM, n = 4 slices) or 6-cyano-7-nitroquinoxaline-2,3-dione/(2R)-amino-5-phosphonovaleric acid (10/40 μM). LFP responses were recorded simultaneously to monitor independently the effect of the receptor antagonists on synaptic transmission. We found that later components of LFPs were consistently blocked by glutamate receptor antagonists; an early component (latency ~1 ms) in response to WM stimulation was resistant to block in some cases and is assumed to represent an antidromic population spike (Fig. 8*A*). LFP responses to V2L stimulation were always completely blocked by glutamate receptor antagonists (not shown). Ca responses of most cells were blocked by GluR antagonists (Fig. 8*B*), though responses in a small number of cells were resistant to block (Fig. 8*B*, asterisks). On average, 85% of responses to WM stimulation and 82% of responses to V2L stimulation were blocked (Fig. 8*C*). These data indicate that most, but not all, Ca responses were due to synaptically driven action potentials, with the remainder presumably due to antidromic or direct stimulation of labeled cells.

Electrophysiological Responses to WM, V2L Stimulation in Au1

To determine the functional effects of the observed projection from V2 to Au1, we recorded whole-cell responses in Au1 to afferent stimulation in layer 5 of V2L and the WM deep to Au1. We reasoned that a descending cortical projection to Au1 would most likely serve as a modulatory input to the cortical column and so compared the response to stimuli applied to the WM alone with responses to V2L stimulation alone and to paired V2L and WM stimulation.

We recorded from 20 pyramidal cells in layers 2–5 of Au1 under whole-cell current clamp. These cells could be classified as regular spiking (n = 18; Fig. 9*Ai*) or intrinsic bursting cells (n = 2). Excitatory postsynaptic potentials (EPSPs) evoked in response to WM stimulation had latencies of 3.07 ± 1.05 ms and in 5 of 11 cells tested could elicit spikes at moderate stimulation intensities. Disynaptic inhibition following WM stimulation was observed in 12 of 16 cells tested (Fig. 9*Aii*). Afferent stimulation applied to V2L elicited EPSPs in 18 of 20 cells tested and were of longer latency (6.46 ± 1.85 ms; Fig. 9*Aiii*) and were superthreshold at higher intensities in 5 of 10 cells tested (not shown). In contrast to WM stimulation, disynaptic inhibition upon stimulation of V2L was observed in only 3 of 18 cells tested. However, 2 additional cells recorded in layers 4 and 5 that responded to V2L stimulation were identified as GABAergic interneurons, in one case based on the cell's nonadapting, fast-spiking pattern common in GABAergic interneurons (Connors and Gutnick 1990) (Fig. 9*Bi*) and in the other case based on its morphology visualized via biocytin injection (not shown). These cells exhibited a small excitatory synaptic response to V2L stimulation (Fig. 9*Biii*); one showed no response to WM stimulation (Fig. 9*Bii*) and other exhibited an EPSP/inhibitory postsynaptic potential sequence (not shown). Interestingly, in the cell illustrated in Figure 9*B*, the synaptic responses to V2L stimulation consistently appeared as triplets of EPSPs, most likely due to bursts fired by the presynaptic cell in V2L.

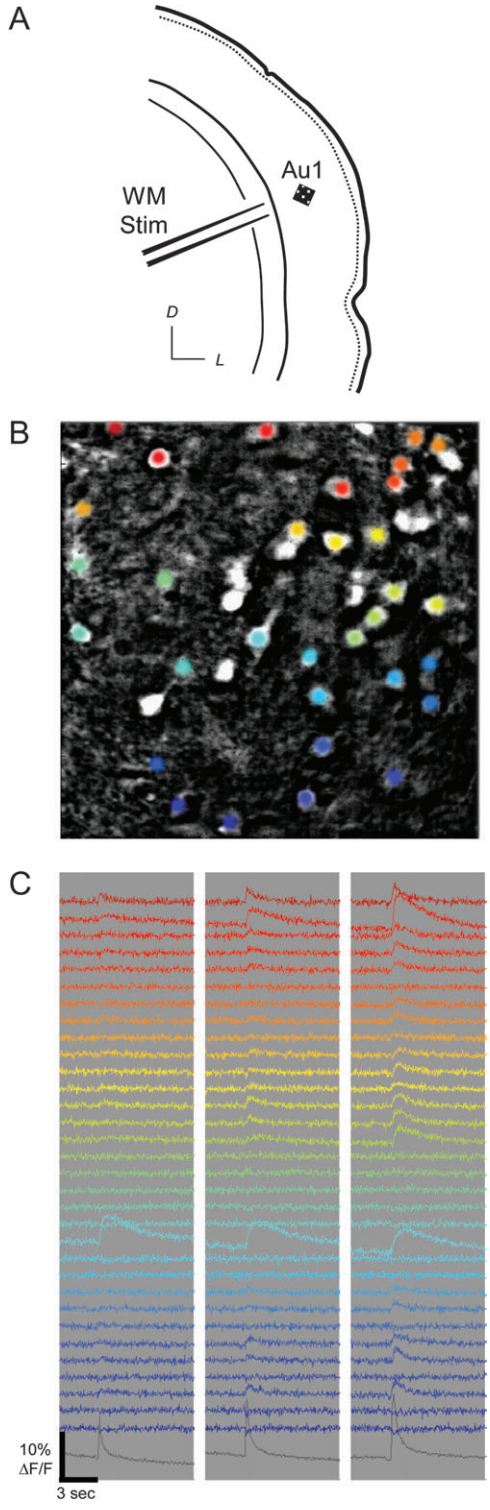

Figure 5. Neural activity monitored in Au1 using Ca imaging. (*A*) Schematic illustration of experimental stimulation and recording arrangement in brain slice. Square indicates orientation of image in (*B*). Orientation vane: D, dorsal; L, lateral. (*B*) Fluorescence in cell bodies labeled with calcium dye OGB-1. Colored cells correspond to matching traces in (*C*). White cells were labeled but unresponsive. Pial surface is toward upper right. Image is 200 μm on each side. (*C*) Calcium traces of individual cell responses to WM stimulation at 2, 4, and 8 pulses at 40 Hz (left, middle, and right columns, respectively). Bottom gray traces show averaged neuropil response.

The ability of V2L inputs to modulate responses to WM stimulation was evaluated by pairing stimuli to the 2 afferent pathways at various delays ranging from –40 to 320 ms (Fig. 9*C*,*D*; same cell as in Fig. 9*A*). In the cell illustrated, for WM stimulus intensities that were always subthreshold, preceding WM stimulation with activation of V2L rendered the WM stimulus superthreshold on all or most trials for delays of 5–8 ms; at negative delays (i.e., with WM preceding V2L stimulation) or at delays ⩾30 ms, no change in spike probability was apparent, while delays between 10 and 30 ms moderately enhanced spiking probability (Fig. 9*C*,*D*).

These electrophysiological data suggest that afferents arising from V2L can modulate spiking activity in Au1. Direct excitation of pyramidal cells by V2L afferents is expected to increase these cells' responsiveness to WM stimuli. Some evidence that V2L afferents also engage inhibitory circuits in Au1 was observed, suggesting that at the network level, modulation of columnar activity in Au1 may be complex and bidirectional. We investigated these circuit interactions at the network level using the Ca imaging technique.

Modulation of Ca Responses to WM Stimulation by Activation of V2L

The ability of V2L afferents to modulate spiking activity in Au1 networks was investigated by labeling cells in Au1 with OGB-1 and comparing the responses to WM and V2L stimulation alone with those in response to paired stimulation. Stimuli consisted of single or short trains of pulses (2–20 pulses at 40 Hz), and paired stimulation was either interleaved (i.e., sequences of V2L–WM pairs, at a fixed delay, applied at 40 Hz) or sequential (i.e., a train applied to V2L at 40 Hz followed at a specific delay by a train applied to WM at 40 Hz). Because we were interested in a priming effect of the V2L projection on the cortical column in Au1, we focused primarily on responses to paired stimuli in which activation of V2L preceded stimulation of the WM.

As mentioned above, WM stimuli typically evoked responses in many more cells compared with stimuli applied to V2L (Fig. 10, compare first and second columns). Because the afferents activated by stimulation in V2L and the WM represent largely nonoverlapping pathways, we expect that the most commonly observed response to paired stimulation would be simple linear summation of the responses to WM and V2L alone: if a cell fires a spike in response to WM stimulation and a spike in response to V2L stimulation, we expect that its response to stimulation of V2L followed by WM would be 2 spikes. Deviation from this simple linear scheme would be superlinear or sublinear interactions between the 2 pathways. For example, if the response to V2L is subthreshold but brings the cell closer to firing threshold, the response to paired stimulation would be superlinear. Conversely, if stimulation of V2L engages inhibitory circuits or leaves the cell in a relative refractory period, the response to paired stimulation may be sublinear. The majority of cells exhibiting responses to WM and V2L stimulation exhibited linear summation to paired stimulation. However, in other cells paired stimulation often elicited responses that deviated from what would be expected by simple linear summation of the responses to WM and V2L stimulation alone. For example, some cells responded to paired stimulation when they showed no response to either stimulus in isolation (Fig. 10, right column, cells marked by asterisks), while other cells showed greatly facilitated responses to paired

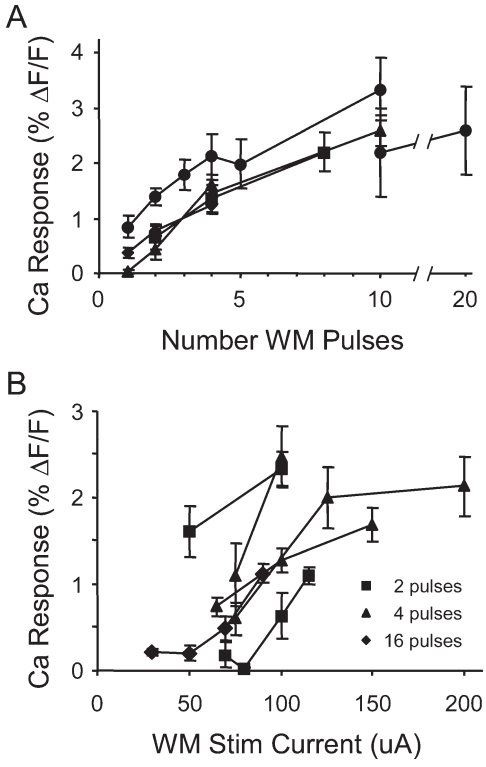

Figure 6. Ca responses are graded with stimulus intensity. (*A*) Relation between number of WM stimulus pulses in a train and Ca response. (*B*) Ca response in relation to WM stimulus intensity. For both (*A*) and (*B*), lines connect data collected in the same experiments. Error bars = ± 1 standard error of the mean for both (*A*) and (*B*).

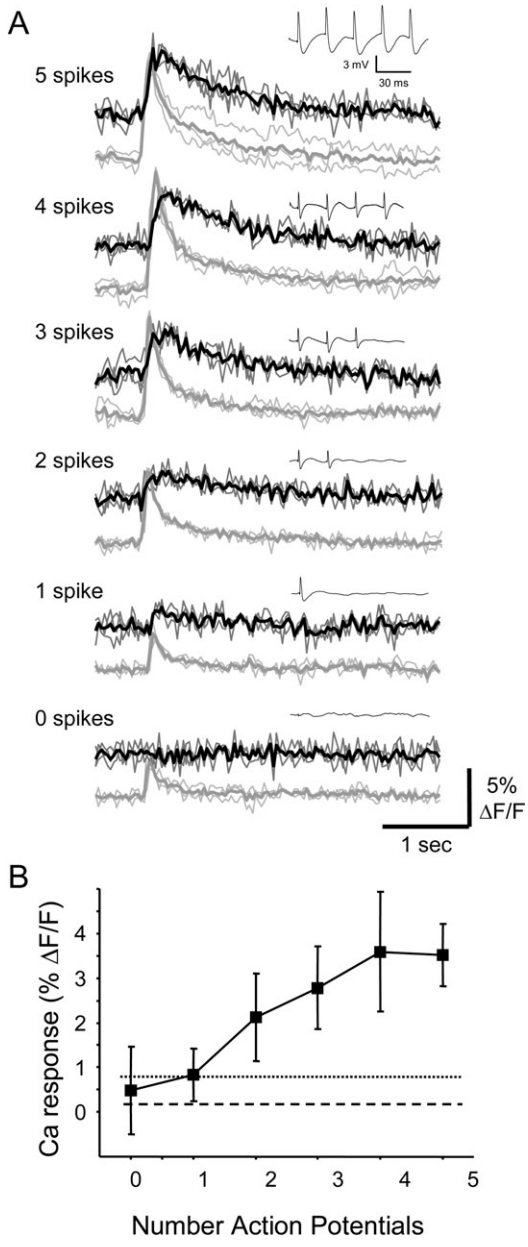

Figure 7. Ca responses in Au1 neurons are triggered by action potentials. (*A*) Fluorescence traces and simultaneously recorded cell-attached patch signals (insets) from a layer 5 pyramidal cell in response to stimulation of WM. An increasing number of spikes fired led to graded increases in the fluorescence response, whereas there was no response in the absence of spikes (bottom traces). Each fluorescence trace is the average (thick line) of 3 trials (thin lines). In each panel, cell responses (upper traces) were corrected for responses in surrounding neuropil (lower traces). Note difference in timescales for fluorescence and electrophysiological signals. (*B*) Summary data across 14 cells show peak fluorescence response amplitude as a function of the number of observed spikes. Error bars correspond to ±SD. Dashed horizontal lines are average response to sham stimulation (i.e., fluorescence response in absence of stimulation). Dotted lines indicate 2SD above the sham average.

stimulation (Fig. 10, right column, cells marked by diamonds). In other experiments, both facilitation and suppression of WM responses by the preceding V2L stimulation were observed (Fig. 11). Thus, activation of V2L can indeed alter the transfer of information through the cortical column in Au1.

Previous work in superior colliculus and multisensory cortex (Stein and Wallace 1996; Wallace et al. 1998) suggests that multisensory interaction is governed by the principle of "inverse effectiveness," in which the interaction depends on the strength of the response to stimuli of one sensory modality alone: the strongest cross-modal enhancements are observed for weak unimodal responses, whereas stimuli that by themselves elicit a strong response are little affected by stimulation in another modality. This principle provides a possible basis for the multisensory enhanced perception of weak stimuli or qualitative altered perception of stimuli that are ambiguous in one modality. We tested whether this principle holds for the modulation of responses in Au1 by comparing the effect of stimulating V2L on WM responses elicited at different intensities (Fig. 12). Consistent with the principle of inverse effectiveness, we found that weak or near-threshold WM responses were more likely to be modulated (typically facilitated; paired *t*-test, $P < 0.02$) by V2L stimulation (Fig. 12). This effect is similar to that observed in our intracellular recordings (Fig. 9), in which stimuli near- but subthreshold are likely to be made superthreshold by preceding V2L excitation. Higher intensity stimuli, which are already superthreshold, will be less affected by V2L excitation since the cells are already spiking in response to WM stimuli alone.

To determine which cells were significantly affected by V2L stimulation, we computed the ratio of the paired response (R_{Pr}) with the response to WM stimulation (R_{WM}) and reasoned that substantial deviation from unity would indicate a significant effect of the preceding V2L stimulation. We used a local false discovery rate analysis (Efron 2004) in which our observed data distribution of R_{Pr}/R_{WM} values (Fig. 13*A*, solid black line), derived from >1400 cells, was compared with a null distribution based on the ratio of sums of WM responses alone, which fit well the central portion of the data distribution (Fig. 13*A*,

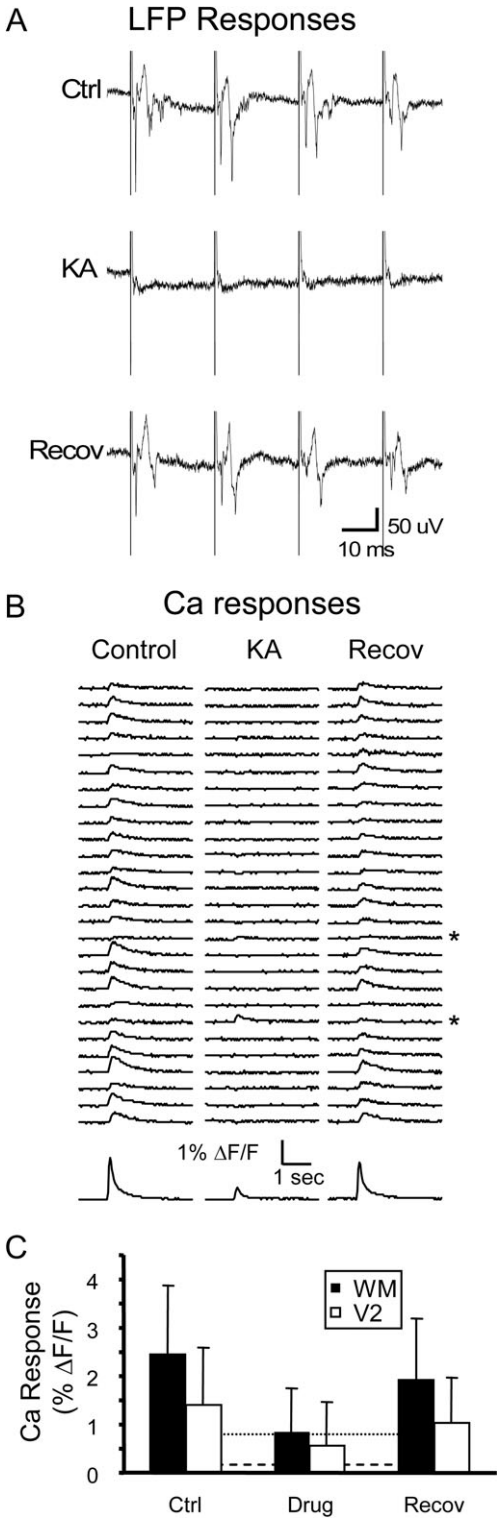

Figure 8. Ca responses in Au1 neurons are primarily synaptically mediated. (*A*) LFP recordings in layer 5 in response to WM stimulation (4 × 40 Hz, 100 μA) before (Ctrl), during (K Acid), and after (Recov) synaptic blockade with 4 mM kynurenic acid. (*B*) Corresponding fluorescence traces from experiment illustrated in (*A*). Responses in all but 2 of these cells were blocked (asterisks), and the effect reversed within 20 min (right column). Traces at bottom illustrate neuropil response. (*C*) Summary data from 8 experiments using either kynurenic acid ($n = 4$) or 6-cyano-7-nitroquinoxaline-2,3-dione/(2R)-amino-5-phosphonovaleric acid ($n = 4$) to block excitatory synaptic transmission in response to WM stimulation (68 cells) and from 7 experiments using 6-cyano-7-nitroquinoxaline-2,3-dione/(2R)-amino-5-phosphonovaleric acid to block responses to V2L stimulation (28 cells). Error bars are SD. Horizontal lines are mean of sham analysis (dashed line, i.e., responses detection algorithm run on data segments in which no stimulus was applied) and sham mean + 2SD (solid line).

dotted black line; see Methods). In the tails of the distributions, the data and null curves diverge, reflecting cells whose WM responses were altered by the preceding V2L stimulation, either via suppression ($R_{Pr}/R_{WM} \ll 1$) or summation ($R_{Pr}/R_{WM} \gg 1$). We chose as a significance criterion a 5-fold difference in observation frequency for the data versus the null distribution (Fig. 13*A*; gray filled area); cells with values of R_{Pr}/R_{WM} in these bins were considered to be significantly affected by preceding V2L stimulation. Based on this method, we estimate that significant interactions between V2L and WM stimuli were observed in 248 of 1417 cells, with 61 cells exhibiting suppression and 187 cells exhibiting summation.

The interactions between V2L and WM stimuli in Au1 and the stronger effects near threshold are summarized in Figure 13*B*,*C*, which plots the difference $R_{Pair} - R_{WM}$ as a function of WM response amplitude (Fig. 13*B*) and V2L response amplitude (Fig. 13*C*) for the same population of cells. Included in this figure are those cells whose Ca responses were $\Delta F/F > 0.78\%$, which in our Ca spike data above represented the threshold for detected spike-evoked responses (Fig. 7). Cells with significant effects of V2L stimulation by the test illustrated in Figure 13*A* are marked with black circles. All other cells are marked with gray circles. Values of $R_{Pair} - R_{WM} < 0$ indicate suppression of the WM response by the preceding V2L stimulation. Values of $R_{Pair} - R_{WM} > 0$ indicate a positive contribution (summation) of the V2L response to the paired response. This contribution can result in sublinear, linear, or superlinear summation, depending on the magnitude of the V2L response (see below). Two important aspects of the data can be gleaned from the plot in Figure 13*B*. First, suppression of WM responses occurs less often than summation. Second, the largest positive values of $R_{Pair} - R_{WM}$ are clustered at small or zero WM responses, consistent with the greatest effect of V2L stimulation being on sub- or near-threshold WM responses.

To interpret values of $R_{Pair} - R_{WM}$ in terms of responses to V2L, we show these difference values as a function of V2L response amplitude (Fig. 13*C*). As in Figure 13*B*, points below the line $R_{Pair} - R_{WM} = 0$ indicate V2L-mediated suppression of the WM response. All points above the dashed line indicate summation of V2L and WM responses. Points clustered along the identity line indicate linear summation, that is, $R_{Pair} = R_{WM} + R_{V2}$. Points above this line indicate superlinear summation, that is, facilitation of the WM response by the preceding V2L stimulus, and points below this line, but above the horizontal 0 line, indicate sublinear summation. Many data points cluster on the identity line, indicating that linear summation is common. Most of the cells exhibiting superlinear summation cluster near zero on the horizontal axis, indicating that V2L stimulation tends to facilitate many cells' responses to WM stimulation even when the cells exhibit zero or small response to V2L alone. This is consistent with our observation using whole-cell recordings that responses to V2L tended to be subthreshold. Similarly, most of the cells exhibiting negative values of $R_{Pair} - R_{WM}$ exhibit small or zero V2L responses, suggesting that V2L activation can engage inhibitory circuits in Au1 with no or little direct excitation of affected cells.

The tendency of the largest effects of paired stimulation to occur in cells with small WM responses is best illustrated in the cumulative amplitude plots of Figure 13*D*. Here, we rank-ordered the data from the entire population of 1417 cells according to increasing WM response amplitude. Each point on the cumulative amplitude curve represents the response amplitude for the cell at that point summed with all the response amplitudes of the cells below that point. For example, point 10 of the WM curve is the

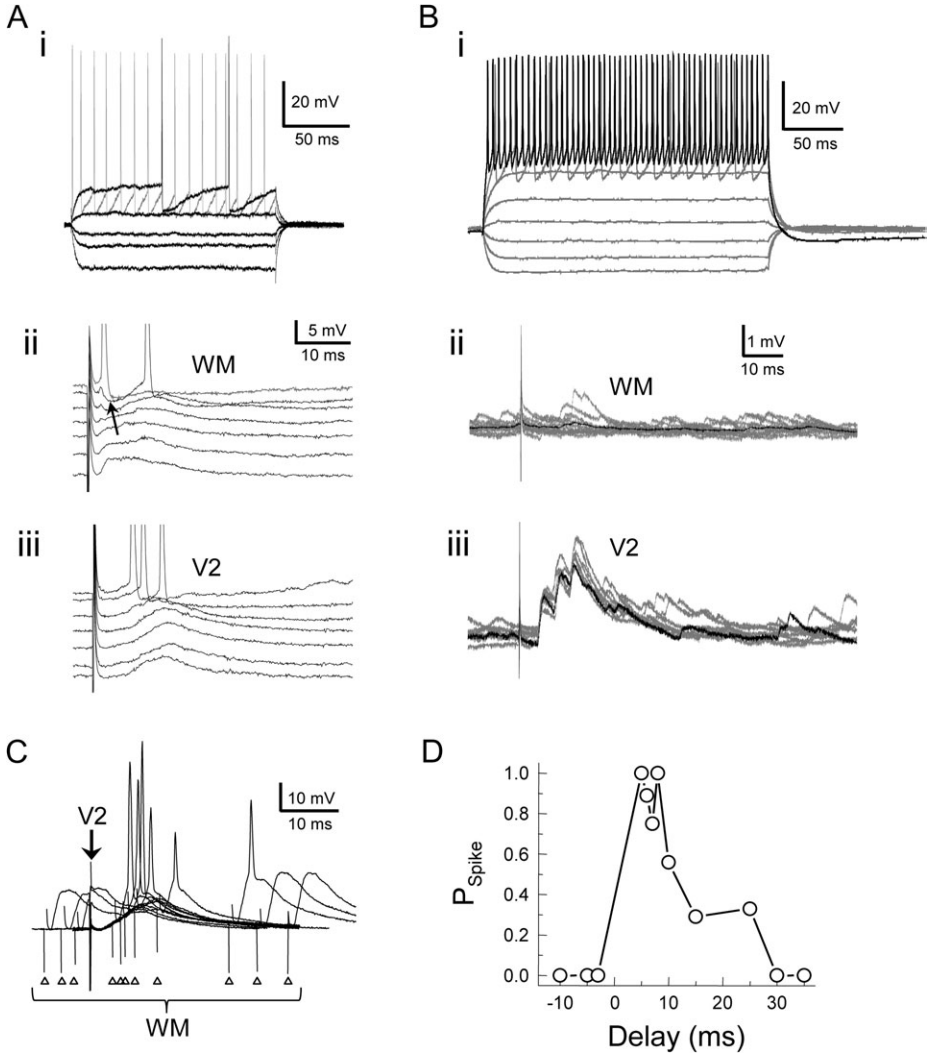

Figure 9. Intracellular recordings from cells responsive to V2 and WM stimulation. (*A*) Responses from a regular spiking layer 3 pyramidal cell to polarizing current pulses (*i*), WM (*ii*), and V2 stimulation (*iii*). In (*ii*) and (*iii*), the cell was held at potentials positive and negative to rest to test for the presence of a disynaptic inhibitory component, which was observed for WM (black arrow) but not V2L stimulation. (*B*) Responses of a fast-spiking (putatively inhibitory) cell to polarizing current pulses (*i*), WM (*ii*), and V2L stimulation (*iii*). In (*ii*) and (*iii*), single trials are shown in gray and average responses are shown in black. (*C*) Recording from the same cell as in (*A*). Here, preceding activation of V2L (arrow) renders WM stimulation (triangles) superthreshold at specific delays. Responses are the average of 10 trials. (*D*) Spike probability as a function of V2 delay for the data in (*C*). Positive delays correspond to V2L stimulation preceding WM stimulation.

sum of the 10 smallest cell responses to WM stimulation. In the associated pair curve, point 10 is the paired response of the same 10 cells used to calculate the WM value.

Cells with the smallest WM response amplitude tend to have the largest values of $R_{Pair} - R_{WM}$, as evidenced by the divergence of the difference curve from the WM amplitude curve for the smallest values of WM response amplitude. As cells with larger and larger WM response amplitudes are incorporated into the cumulative plot (i.e., proceeding from left to right in Fig. 13*D*), the difference curve begins to flatten out as more and more cells exhibit small values of $R_{Pair} - R_{WM}$. This figure also shows that the dominant effect of V2L stimulation was summation as the cumulative paired response is much larger than the cumulative WM response.

Discussion

Summary

We have shown that a descending projection from extrastriate visual to primary auditory cortex in mice is capable of modulating responses in Au1 to WM stimuli. In vivo and in vitro anterograde labeling showed that the projection from V2 to Au1 terminated with highest density in supragranular and infragranular layers, a pattern that is complementary to the ascending lemniscal thalamocortical projection from the medial geniculate (Caviness and Frost 1980; Frost and Caviness 1980) and is consistent with the termination patterns of other descending corticocortical projections (Shi and Cassell 1997). Electrophysiological data suggest that fibers from V2L synapse onto both pyramidal neurons and GABAergic interneurons in Au1 and can modulate the responses to stimulation of the WM. Our Ca imaging data show that spiking patterns in large numbers of cells in Au1 are altered by preceding stimulation of V2L. Paired responses most commonly exhibited some form of summation, and this effect tended to be most pronounced for small, near-threshold WM stimuli. Suppression of WM responses was also observed. This is the first demonstration that activation of a specific visual area can modulate responses in primary auditory cortex.

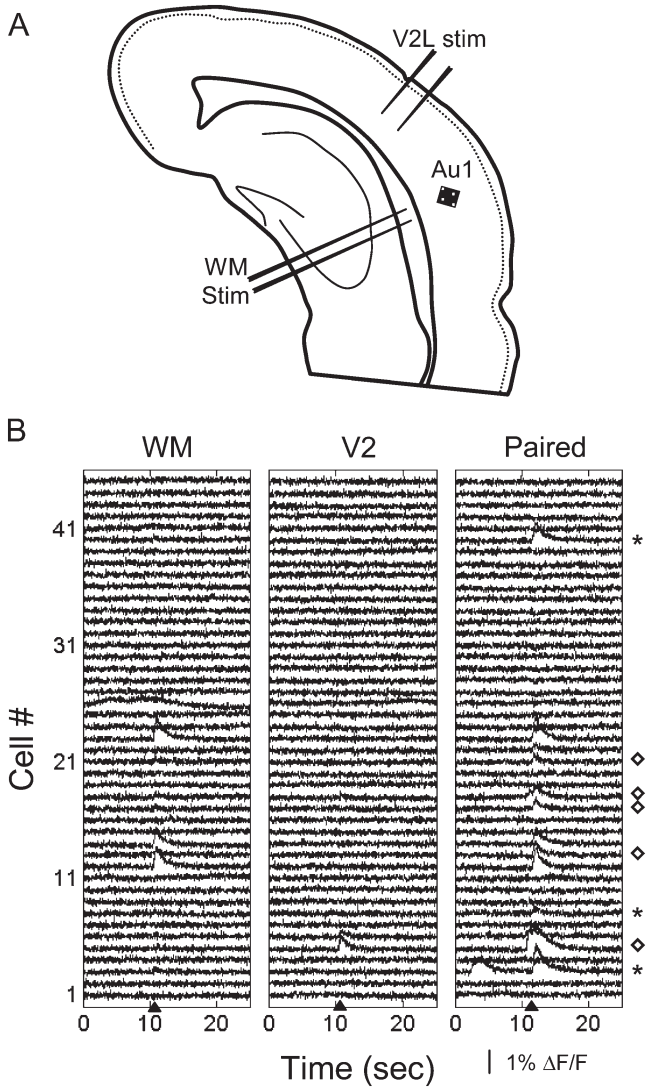

Figure 10. Modulation of Ca responses to WM stimuli by V2. (*A*) Cartoon of a brain slice showing experimental preparation. The square (200 × 200 μm) indicates the approximate area that was imaged in (*B*). Stimulating electrodes were placed in V2L and in the WM. (*B*) Fluorescence traces recorded from 45 cells in response to stimulation in the WM (left column; 125 μA, 10 pulses at 40 Hz), V2L (middle column; 250 μA, 10 pulses at 40 Hz), or both (right column; V2L stimulus train preceded WM stimulus train by 25 ms). Stimuli were applied at times indicated by arrowheads. Note that some cells responded to paired stimulation when they showed no response to either WM or V2L stimulus in isolation (asterisks), while other cells showed greatly facilitated responses to paired stimulation (diamonds).

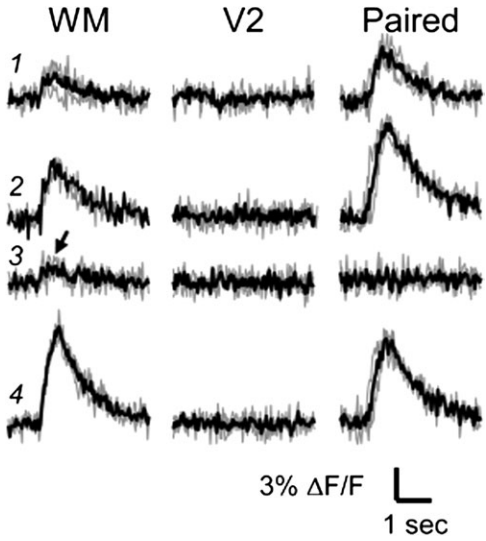

Figure 11. Ca responses to WM stimulation can be facilitated or suppressed by V2 stimulation. Fluorescence traces recorded simultaneously from 4 representative cells in Au1 in response to WM (left; 100 μA, 4 pulses at 40 Hz), V2L (middle; 200 μA, 4 pulses at 40 Hz), and paired (right; V2L and WM stimulus trains interleaved, V2L stimuli preceded WM stimuli by 25 ms) stimulation. "Dark traces" are averages of 3 trials (gray traces). All 4 cells exhibit responses to WM stimulation (small response in third cell is marked by arrow). None exhibited responses to V2L stimulation but with paired stimulation WM responses in top 3 cells were modulated: 2 were facilitated (cells 1 and 2) and 1 was suppressed (cell 3). The bottom cell was unaffected. All comparisons via Student's *t*-tests with significance criterion $P < 0.05$.

Potential Limitations

An inherent limitation of using electrical stimuli applied to brain slices is the possibility of activating fibers of passage that originate in other brain areas. The scenario of greatest concern in the present study is the possibility that stimulation in V2L antidromically activated cells projecting from Au1 to V2L and that the synaptically driven responses that we observed were due to a dense plexus of local collaterals in Au1 from these backfired cells. Indirect evidence for antidromically activated cells in Au1 is found in Figure 8, in which a small percentage of responses to V2L stimulation were not blocked by glutamate receptor antagonists. In spite of this observation, however, we saw little anatomical or electrophysiological evidence for this scenario, as discussed below. By contrast, we did observe evidence for a strong projection from V2L to Au1, and the possibility that these terminals in Au1 were actually local collaterals of cells in Au1 that project to V2L and whose axons and terminals in Au1 were retrogradely labeled in the absence of labeling in their cell bodies is exceedingly unlikely. Thus, we believe that any such confounding responses are unlikely to contribute importantly to the results presented here.

Projection from Visual to Auditory Cortex

Multimodal integration in neocortex is likely important for forming global percepts, and it has become increasingly evident that this process is distributed across the cortical hierarchy. We show here evidence for such integrative mechanisms in primary auditory cortex of mice. Our findings are consistent with previous anatomical work using retrograde tracers (Budinger et al. 2006; Bizley et al. 2007) and physiological experiments in primary auditory cortex (Fu et al. 2003; Ghazanfar et al. 2005; Lakatos et al. 2005, 2007, 2009; Budinger et al. 2006; Bizley et al. 2007; Martuzzi et al. 2007; Kayser et al. 2008; Liang et al. 2008). The present paper extends those findings to show that V2L is directly involved in modulation of responses in Au1.

The laminar profile of the projection's terminal distribution is typical for "feedback" or modulatory cortical connections (Felleman and Van Essen 1991; Johnson and Burkhalter 1997), with the terminal density highest in supragranular and infragranular layers (Figs 1–4), a pattern observed previously in rat (Smith et al. 2010) and suggested in gerbil (Budinger et al. 2006). Similarly, extrastriate visual cortex projects to caudal auditory cortical areas in macaque (Smiley and Falchier 2009; Falchier et al. 2010), and these projections arise in infragranular layers and activate superficial and deep layers (Schroeder and Foxe 2002). This projection pattern appears

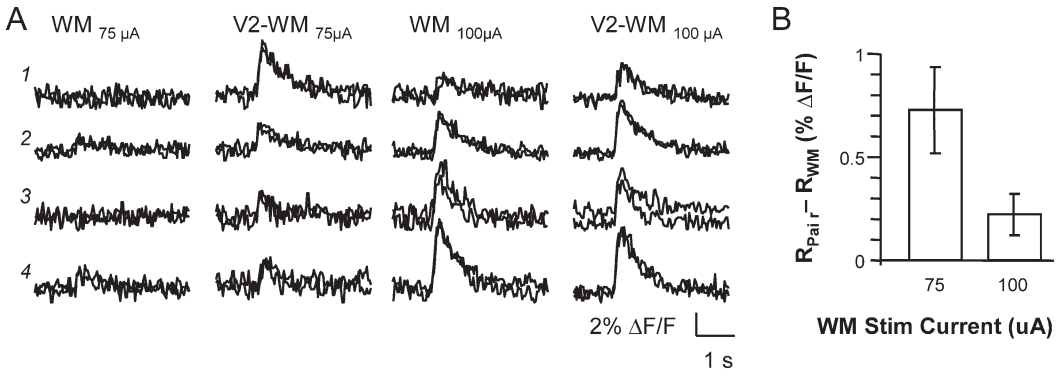

Figure 12. Facilitation by V2 stimulation is more effective for small WM responses. (*A*) Fluorescence traces recorded from 4 representative cells simultaneously in Au1 in response to WM (first and third columns), paired V2L–WM (second and fourth columns) stimulation for 2 different WM stimulation intensities: 75 μA (first and second columns) and 100 μA (third and fourth columns). V2L stimulation intensity was identical in both cases (200 μA). Four pulses each were applied to WM and V2L, at 0 ms delay. Note that for the lower WM stimulation intensity, all 4 cells exhibit facilitation in response to paired stimulation, but for the higher WM stimulation intensity, this is true only for cells 1 and 2. (*B*) Summary of all recordings from the experiment in (*A*) (mean ± standard error of the mean; $n = 30$ cells) showing the difference between response amplitude (%ΔF/F) to paired stimulation versus WM alone. Note greater facilitation (i.e., greater difference) for smaller WM stimulation intensity.

to be common across sensory modalities, as somatosensory input to auditory cortex in monkeys generates current sinks in infragranular and supragranular layers (Lakatos et al. 2007), and a reciprocal feedback projection arises from belt and parabelt auditory areas to V1 and V2 (Falchier et al. 2002; Rockland and Ojima 2003; Hall and Lomber 2008). These descending projections are complementary to the lemniscal thalamic projection from the medial geniculate (Romanski and LeDoux 1993; Cruikshank et al. 2002; Kimura et al. 2003) but overlap projections from extralemnical thalamic nuclei (Linke and Schwegler 2000; Kimura et al. 2003; Smith et al. 2010). The functional implications of these projection patterns are discussed below.

Ca Responses in Au1

The Ca imaging technique that we employed has been used successfully both in vivo and in vitro to monitor neural activity in cortical circuits (Stosiek et al. 2003; Kerr et al. 2005). As in these previous studies, labeled cells were predominantly neurons. In 14 whole-cell and on-cell patch-clamp recordings from labeled cells, we never observed a cell that did not fire an action potential in response to synaptic stimulation of sufficient intensity or in response to depolarizing current injection. We did occasionally observe cells whose Ca response to synaptic stimulation was much slower than other cells and/or which exhibited slow spontaneous Ca transients, and these cells were assumed to be glial cells, as reported previously (Kerr et al. 2005). However, they represented ~0.1% of the total cells observed with Ca responses.

We show that Ca responses to afferent stimulation were primarily due to synaptically driven action potentials. In on-cell recordings from labeled cells, we could detect Ca responses to afferent stimulation on single trials reliably when cells fired single action potentials but not when stimuli were subthreshold. In a minority of cells, averaged responses revealed small, subthreshold Ca responses, presumably representing Ca transients in response to activation of voltage- or ligand-gated channels by depolarizing EPSPs. Using glutamate receptor antagonists, we show that spikes in response to afferent stimulation were primarily synaptically driven, with Ca responses blocked in >80% of cells. Responses in cells that were resistant to blockade of glutamate receptors most likely could be explained by 1 of 2 possibilities: either incomplete block of synaptic glutamate receptors in those cells or spiking due to antidromic activation or direct stimulation of dendritic processes. The latter possibilities are not surprising for WM stimuli as corticothalamic and corticofugal cells send their axons through the WM to reach their targets. In our experiments, LFP responses to WM stimulation often had a short latency component that was not blocked by glutamate receptor antagonists, and antidromic responses to WM stimulation were observed (though were rare, especially at low stimulus intensities). In contrast, antidromic activation of cells in Au1 by stimulation in V2L is unexpected, as the projection from Au1 to V2L is reported to be weak (Mascagni et al. 1993; Shi and Cassell 1997), and we observed only a single retrogradely labeled cell in Au1 after injecting biocytin into V2L in vitro, though numerous cells were observed in V2M and V1. In 22 whole-cell recordings from cells in Au1, we observed an antidromic response to V2L stimulation only once, and LFP responses to V2L stimulation were completely blocked by glutamate receptor antagonists. It should be noted that our electrophysiological data indicate that most responses to V2L stimulation are subthreshold, indicating that if resistant cells were being activated antidromically, the overall percentage of cells exhibiting antidromic responses is much smaller than suggested by these Ca imaging results, in which only superthreshold responses are monitored.

Modulation of Au1 Responses by Visual Stimuli

We have shown that preceding activation of V2L could alter subsequent responses to WM stimuli. In our electrophysiological experiments, we show that the optimal timing for activation of V2L relative to the WM was 5–10 ms, similar to the difference in synaptic delay between the 2 inputs (Fig. 10). This is consistent with previous studies that showed that heteromodal stimuli are most effective at modulating responses if they precede or overlap auditory stimuli (Ghazanfar et al. 2005; Bizley et al. 2007; Lakatos et al. 2007; Kayser et al. 2008). These previous studies have also shown that heteromodal stimuli can either enhance or suppress auditory responses depending on the specific relative timing, consistent with our observation of bidirectional modulation of responses to WM stimuli by stimulation of V2L; in most cases, responses to V2L

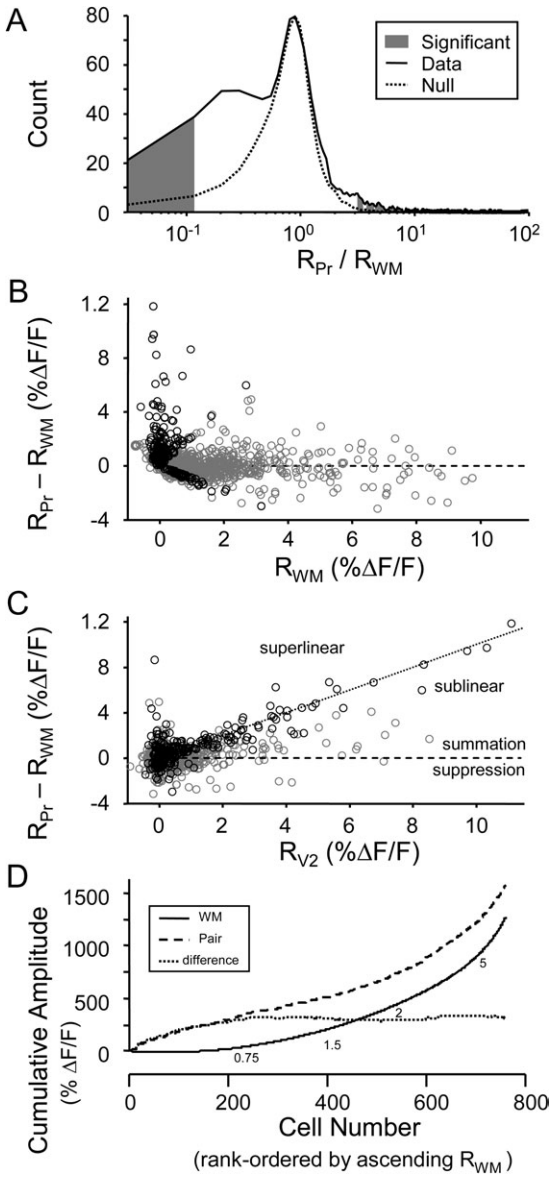

Figure 13. Summary of effects of V2 stimulation on WM responses. (*A*) Statistical analysis of responses to determine cells whose WM responses were significantly affected by preceding V2L stimulus. The data distribution (solid line) consists of the ratio of mean paired to mean WM response amplitude in all cells with detected responses to WM, V2L, or paired stimulation ($n = 1417$ cells). Ratio values near unity arise from cells with no significant difference between paired and WM alone. Ratio values in the tails of the distribution arise from cells with significant differences. To distinguish between these 2 populations in the data distribution, a null distribution (dotted line) was created from the WM-alone responses and a local false discovery rate analysis was used to determine which values of the ratio were significantly different from unity (gray filled area). (*B*) Each point represents the difference between the responses to paired stimulation and WM alone ($R_{Pr} - R_{WM}$) plotted versus the amplitude of the WM response (R_{WM}) in a single cell. Zero difference indicates no effect of V2L stimulation. Values <0 indicate suppression of WM response by preceding V2L stimulation, while values >0 indicate summation, due to either enhancement of WM response (in the absence of response to V2L alone) or additive effects of V2L and WM responses. (*C*) $R_{Pr} - R_{WM}$ plotted versus the amplitude of the V2L response (R_{V2L}) in the same cell, for the same population of cells as in (*A*). Values below the horizontal line ($R_{Pr} - R_{WM} = 0$) indicate suppression and those above the line indicate summation. The identity line indicates linear summation. Values above the identity line indicate superlinear summation, while values below the line indicate sublinear summation. For panels (*B*) and (*C*), cells whose paired responses were significantly different from WM responses by the analysis of panel (*A*) are marked with "black circles." All other cells are marked with "gray circles." (*D*) Cumulative amplitude plots for the data in (*B*) and (*C*). All cells, both those whose WM responses were significantly affected by V2L stimulation and those that were not, are included. The increasing difference between the paired and WM curves at low WM response amplitude reflects the tendency of V2L stimulation to have the greatest effect on small-amplitude WM responses. Numbers below the WM curve indicate at what point in the distribution of cells the indicated WM response amplitude occurred. In all panels, only cells with responses of $\Delta F/F > 0.78$ % to WM, V2L, and/or paired stimulation were included.

stimuli summed with responses to WM stimuli but in some cases suppressed these responses (Figs 10–13). We observed summation more frequently than suppression, and we observed more anatomical and physiological evidence for excitatory versus inhibitory effects of V2L stimulation. For example, in only 3 cells of 18 tested did we observe disynaptic inhibition in electrophysiological responses to V2L stimulation. In addition, all V2L terminals were GABA immunonegative, and most (8/9) of these terminals were observed to contact GABA immunonegative postsynaptic structures. The predominance of excitatory effects is consistent with the properties of feedback connections in the visual cortical pathway, in which extrastriate inputs to V1 are primarily excitatory, with little activation of inhibitory circuits (Johnson and Burkhalter 1997). However, other studies have stressed the importance of subthreshold integration and the engagement of inhibitory processes by stimuli from other modalities (Dehner et al. 2004; Meredith and Allman 2009).

Multimodal integration is thought to have the most relevance for detection and processing of weak stimuli (Stein et al. 1993; Wallace et al. 1998; Lakatos et al. 2007). We observed that for both summating and suppressive interactions, V2L stimuli were most effective in altering WM responses that were near threshold (Figs 12–13). These data are consistent with the idea that heteromodal activation of both excitatory and inhibitory circuits serves to boost detectability. This observation may be relevant to the current debate about the functional role of heteromodal inputs, which may serve only to enhance the detectability of sensory stimuli (e.g., Lakatos et al. 2008; Schroeder et al. 2008) or may contribute specific information about the sensory stimulus and thus alter the encoding process itself (e.g., Kayser et al. 2010). The stimuli used in our experiments do not lend themselves easily to studying changes in information coding, but future experiments with more complicated patterns of afferent stimulation may shed light on this debate.

Laminar Dependence

Information from diverse sources is integrated in the cortical column. Due to the laminar organization of afferents and cell types, this integration is likely to occur at the cellular level in only select cell populations, while other cell types may participate in this integration process via circuit and polysynaptic mechanisms. The dendrites of layer 5 corticofugal and corticocallosal pyramidal neurons traverse both thalamorecipient layers and layers receiving descending inputs and are likely loci for integration of these 2 input sources (White and Hersch 1982; Mitani and Shimokouchi 1985; Games and Winer 1988; Hubener and Bolz 1988; Gil and Amitai 1996; Winer and Prieto 2001; Doucet et al. 2003; Tsiola et al. 2003; Christophe et al. 2005; Verbny et al. 2006; Le Be et al. 2007). For this reason, we focused the majority of our experiments on cells in layer 5 in an effort to understand this integration process. We

found that both regular spiking and intrinsically bursting pyramidal cells in layer 5 received excitatory input from V2L. Our experiments were not designed to determine the laminar dependence of responses in Au1 to V2L stimulation as the majority of imaging experiments were performed with a high-power (×40) objective whose limited field of view did not allow comparisons across layers. It was interesting that we could observe responses to V2L stimulation in all layers tested (layers 3–6), suggesting that the influence of this projection is widespread within the column, even though the projection exhibits a strong laminar dependence. Indeed, experiments in vivo have shown a strong heteromodal response in supragranular layers with latency and amplitude comparable to the response in infragranular layers (Schroeder and Foxe 2002; Lakatos et al. 2007). Future experiments with lower power objectives and more standardized stimulation protocols will allow us to map the laminar dependence of the strength of this modulation.

Functional Implications

The complementary ascending and descending projections to sensory neocortex are postulated to underlie comparisons of expected and observed sensory events, with descending projections carrying predicted activity based on context, experience, and inputs from other modalities and ascending connections carrying current sensory input (Hawkins and Blakeslee 2005; Bar 2009). Thus, descending cortical inputs could prime the column for expected ascending information and could generate distinct responses should the inputs match or diverge from expectations. We have shown that this integration process is complex and nonlinear. It is most effective at near-threshold stimuli for both summing or facilitative modulation and suppressive modulation. These observations raise the intriguing possibility that descending projections do not simply pre-excite the cortical column and enhance responses regardless of the layer and cell type. Mixed facilitative and suppressive as well as subtype-specific effects of V2L stimulation could change the participation of selected cells and circuits within the column in response to ascending input. Such changes in network composition could have broad implications for subsequent processing of the sensory input and the motor patterns that the stimulus triggers. For example, facilitation of cells whose primary outputs are subcortical and engage motor circuits while suppression of cells whose primary outputs are corticocortical may decrease response latency to multimodal inputs of particular behavioral relevance. Such bidirectional modulation may also impact the relative importance of corticocortical versus corticothalamocortical pathways, which arise from distinct cell types within the cortical column (Hallman et al. 1988; Kasper et al. 1994; Lee and Sherman 2010). Demonstrating the existence of such specificity awaits future experiments.

Funding

National Institutes of Health (Bethesda, MD) (DC006013 to M. I. B.); Department of Anesthesiology (233-DS71 to M. I. B.) and School of Medicine and Public Health (233-PRJ39MN to D. J. U.), University of Wisconsin, Madison, WI.

Notes

The authors thank Yakov Verbny (Associate Researcher, Department of Anesthesiology), Nima Ghitani (Research Assistant, Neuroscience Training Program), and Anna Kowalkowski (Research Specialist, Department of Anatomy) for technical support on this project. *Conflicts of Interest* : None declared.

References

Adams JC. 1981. Heavy metal intensification of DAB-based HRP reaction product. J Histochem Cytochem. 29(6):775.

Arnault P, Roger M. 1990. Ventral temporal cortex in the rat: connections of secondary auditory areas Te2 and Te3. J Comp Neurol. 302(1):110–123.

Bar M. 2009. The proactive brain: memory for predictions. Philos Trans R Soc Lond B Biol Sci. 364(1521):1235–1243.

Bizley JK, Nodal FR, Bajo VM, Nelken I, King AJ. 2007. Physiological and anatomical evidence for multisensory interactions in auditory cortex. Cereb Cortex. 17(9):2172–2189.

Budinger E, Heil P, Hess A, Scheich H. 2006. Multisensory processing via early cortical stages: connections of the primary auditory cortical field with other sensory systems. Neuroscience. 143(4):1065–1083.

Calvert GA, Bullmore ET, Brammer MJ, Campbell R, Williams SC, McGuire PK, Woodruff PW, Iversen SD, David AS. 1997. Activation of auditory cortex during silent lipreading. Science. 276(5312):593–596.

Caviness VS, Jr. 1975. Architectonic map of neocortex of the normal mouse. J Comp Neurol. 164(2):247–263.

Caviness VS, Jr, Frost DO. 1980. Tangential organization of thalamic projections to the neocortex in the mouse. J Comp Neurol. 194(2):335–367.

Christophe E, Doerflinger N, Lavery DJ, Molnar Z, Charpak S, Audinat E. 2005. Two populations of layer V pyramidal cells of the mouse neocortex: development and sensitivity to anesthetics. J Neurophysiol. 94(5):3357–3367.

Clerici WJ, Coleman JR. 1990. Anatomy of the rat medial geniculate body: I. Cytoarchitecture, myeloarchitecture, and neocortical connectivity. J Comp Neurol. 297(1):14–31.

Connors BW, Gutnick MJ. 1990. Intrinsic firing patterns of diverse neocortical neurons. Trends Neurosci. 13(3):99–104.

Contreras D, Llinas R. 2001. Voltage-sensitive dye imaging of neocortical spatiotemporal dynamics to afferent activation frequency. J Neurosci. 21(23):9403–9413.

Cruikshank SJ, Killackey HP, Metherate R. 2001. Parvalbumin and calbindin are differentially distributed within primary and secondary subregions of the mouse auditory forebrain. Neuroscience. 105(3):553–569.

Cruikshank SJ, Rose HJ, Metherate R. 2002. Auditory thalamocortical synaptic transmission in vitro. J Neurophysiol. 87(1):361–384.

Dehner LR, Keniston LP, Clemo HR, Meredith MA. 2004. Cross-modal circuitry between auditory and somatosensory areas of the cat anterior ectosylvian sulcal cortex: a 'new' inhibitory form of multisensory convergence. Cereb Cortex. 14(4):387–403.

Doucet JR, Molavi DL, Ryugo DK. 2003. The source of corticocollicular and corticobulbar projections in area Te1 of the rat. Exp Brain Res. 153(4):461–466.

Driver J, Noesselt T. 2008. Multisensory interplay reveals crossmodal influences on 'sensory-specific' brain regions, neural responses, and judgments. Neuron. 57(1):11–23.

Efron B. 2004. Large-scale simultaneous hypothesis testing: the choice of a null hypothesis. J Am Stat Assoc. 99(465):96–104.

Engel AK, Fries P, Singer W. 2001. Dynamic predictions: oscillations and synchrony in top-down processing. Nat Rev Neurosci. 2(10):704–716.

Falchier A, Clavagnier S, Barone P, Kennedy H. 2002. Anatomical evidence of multimodal integration in primate striate cortex. J Neurosci. 22(13):5749–5759.

Falchier A, Schroeder CE, Hackett TA, Lakatos P, Nascimento-Silva S, Ulbert I, Karmos G, Smiley JF. 2010. Projection from visual areas V2 and prostriata to caudal auditory cortex in the monkey. Cereb Cortex. 20(7):1529–1538.

Felleman DJ, Van Essen DC. 1991. Distributed hierarchical processing in the primate cerebral cortex. Cereb Cortex. 1(1):1–47.

Franklin KBJ, Paxinos G. 2008. The mouse brain in stereotaxic coordinates. Amsterdam: Academic Press.

Frost DO, Caviness VS Jr. 1980. Radial organization of thalamic projections to the neocortex in the mouse. J Comp Neurol. 194(2):369–393.
Fu KMG, Johnston TA, Shah AS, Arnold L, Smiley J, Hackett TA, Garraghty PE, Schroeder CE. 2003. Auditory cortical neurons respond to somatosensory stimulation. J Neurosci. 23(20):7510–7515.
Galaburda AM, Pandya DN. 1983. The intrinsic architectonic and connectional organization of the superior temporal region of the rhesus monkey. J Comp Neurol. 221(2):169–184.
Games KD, Winer JA. 1988. Layer V in rat auditory cortex: projections to the inferior colliculus and contralateral cortex. Hear Res. 34(1):1–25.
Ghazanfar AA, Maier JX, Hoffman KL, Logothetis NK. 2005. Multisensory integration of dynamic faces and voices in rhesus monkey auditory cortex. J Neurosci. 25(20):5004–5012.
Ghazanfar AA, Schroeder CE. 2006. Is neocortex essentially multisensory? Trends Cogn Sci. 10(6):278–285.
Gil Z, Amitai Y. 1996. Properties of convergent thalamocortical and intracortical synaptic potentials in single neurons of neocortex. J Neurosci. 16(20):6567–6578.
Hall AJ, Lomber SG. 2008. Auditory cortex projections target the peripheral field representation of primary visual cortex. Exp Brain Res. 190(4):413–430.
Hallman LE, Schofield BR, Lin CS. 1988. Dendritic morphology and axon collaterals of corticotectal, corticopontine, and callosal neurons in layer V of primary visual cortex of the hooded rat. J Comp Neurol. 272(1):149–160.
Hawkins J, Blakeslee S. 2005. On intelligence. New York: Henry Holt & Co.
Hefti BJ, Smith PH. 2000. Anatomy, physiology, and synaptic responses of rat layer V auditory cortical cells and effects of intracellular GABA(A) blockade. J Neurophysiol. 83(5):2626–2638.
Herbert H, Aschoff A, Ostwald J. 1991. Topography of projections from the auditory cortex to the inferior colliculus in the rat. J Comp Neurol. 304(1):103–122.
Herkenham M. 1980. Laminar organization of thalamic projections to the rat neocortex. Science. 207(4430):532–535.
Heumann D, Leuba G, Rabinowicz T. 1977. Postnatal development of the mouse cerebral neocortex. II. Quantitative cytoarchitectonics of visual and auditory areas. J Hirnforsch. 18(6):483–500.
Hirokawa J, Bosch M, Sakata S, Sakurai Y, Yamamori T. 2008. Functional role of the secondary visual cortex in multisensory facilitation in rats. Neuroscience. 153(4):1402–1417.
Huang CL, Winer JA. 2000. Auditory thalamocortical projections in the cat: laminar and areal patterns of input. J Comp Neurol. 427(2):302–331.
Hubener M, Bolz J. 1988. Morphology of identified projection neurons in layer 5 of rat visual cortex. Neurosci Lett. 94(1–2):76–81.
Johnson RR, Burkhalter A. 1997. A polysynaptic feedback circuit in rat visual cortex. J Neurosci. 17(18):7129–7140.
Kasper EM, Larkman AU, Lubke J, Blakemore C. 1994. Pyramidal neurons in layer 5 of the rat visual cortex. I. Correlation among cell morphology, intrinsic electrophysiological properties, and axon targets. J Comp Neurol. 339(4):459–474.
Katz LC, Burkhalter A, Dreyer WJ. 1984. Fluorescent latex microspheres as a retrograde neuronal marker for in vivo and in vitro studies of visual cortex. Nature. 310(5977):498–500.
Kayser C, Logothetis NK, Panzeri S. 2010. Visual enhancement of the information representation in auditory cortex. Curr Biol. 20(1):19–24.
Kayser C, Petkov CI, Augath M, Logothetis NK. 2007. Functional imaging reveals visual modulation of specific fields in auditory cortex. J Neurosci. 27(8):1824–1835.
Kayser C, Petkov CI, Logothetis NK. 2008. Visual modulation of neurons in auditory cortex. Cereb Cortex. 18(7):1560–1574.
Kerr JN, Greenberg D, Helmchen F. 2005. Imaging input and output of neocortical networks in vivo. Proc Natl Acad Sci U S A. 102(39):14063–14068.
Kimura A, Donishi T, Sakoda T, Hazama M, Tamai Y. 2003. Auditory thalamic nuclei projections to the temporal cortex in the rat. Neuroscience. 117(4):1003–1016.
Lakatos P, Chen CM, O'Connell MN, Mills A, Schroeder CE. 2007. Neuronal oscillations and multisensory interaction in primary auditory cortex. Neuron. 53(2):279–292.
Lakatos P, Karmos G, Mehta AD, Ulbert I, Schroeder CE. 2008. Entrainment of neuronal oscillations as a mechanism of attentional selection. Science. 320(5872):110–113.
Lakatos P, O'Connell MN, Barczak A, Mills A, Javitt DC, Schroeder CE. 2009. The leading sense: supramodal control of neurophysiological context by attention. Neuron. 64(3):419–430.
Lakatos P, Shah AS, Knuth KH, Ulbert I, Karmos G, Schroeder CE. 2005. An oscillatory hierarchy controlling neuronal excitability and stimulus processing in the auditory cortex. J Neurophysiol. 94(3):1904–1911.
Le Be JV, Silberberg G, Wang Y, Markram H. 2007. Morphological, electrophysiological, and synaptic properties of corticocallosal pyramidal cells in the neonatal rat neocortex. Cereb Cortex. 17(9):2204–2213.
Lee CC, Sherman SM. 2010. Drivers and modulators in the central auditory pathways. Front Neurosci. 4:79.
Liang M, van Leeuwen TM, Proulx MJ. 2008. Propagation of brain activity during audiovisual integration. J Neurosci. 28(36): 8861–8862.
Linke R, Schwegler H. 2000. Convergent and complementary projections of the caudal paralaminar thalamic nuclei to rat temporal and insular cortex. Cereb Cortex. 10(8):753–771.
Macaluso E. 2006. Multisensory processing in sensory-specific cortical areas. Neuroscientist. 12(4):327–338.
Martuzzi R, Murray MM, Michel CM, Thiran JP, Maeder PP, Clarke S, Meuli RA. 2007. Multisensory interactions within human primary cortices revealed by BOLD dynamics. Cereb Cortex. 17(7):1672–1679.
Mascagni F, McDonald AJ, Coleman JR. 1993. Corticoamygdaloid and corticocortical projections of the rat temporal cortex: a Phaseolus vulgaris leucoagglutinin study. Neuroscience. 57(3):697–715.
McGurk H, MacDonald J. 1976. Hearing lips and seeing voices. Nature. 264(5588):746–748.
Meredith MA, Allman BL. 2009. Subthreshold multisensory processing in cat auditory cortex. Neuroreport. 20(2):126–131.
Meredith MA, Allman BL, Keniston LP, Clemo HR. 2009. Auditory influences on non-auditory cortices. Hear Res. 258(1–2):64–71.
Merriam EB, Netoff TI, Banks MI. 2005. Bistable network behavior of layer interneurons in auditory cortex. J Neurosci. 25(26):6175–6186.
Metherate R, Cruikshank SJ. 1999. Thalamocortical inputs trigger a propagating envelope of gamma-band activity in auditory cortex in vitro. Exp Brain Res. 126(2):160–174.
Miller MW, Vogt BA. 1984. Direct connections of rat visual cortex with sensory, motor, and association cortices. J Comp Neurol. 226(2):184–202.
Mitani A, Shimokouchi M. 1985. Neuronal connections in the primary auditory cortex: an electrophysiological study in the cat. J Comp Neurol. 235(4):417–429.
Mitani A, Shimokouchi M, Itoh K, Nomura S, Kudo M, Mizuno N. 1985. Morphology and laminar organization of electrophysiologically identified neurons in the primary auditory cortex in the cat. J Comp Neurol. 235(4):430–447.
Murray MM, Molholm S, Michel CM, Heslenfeld DJ, Ritter W, Javitt DC, Schroeder CE, Foxe JJ. 2005. Grabbing your ear: rapid auditory-somatosensory multisensory interactions in low-level sensory cortices are not constrained by stimulus alignment. Cereb Cortex. 15(7):963–974.
Olavarria J, Montero VM. 1989. Organization of visual cortex in the mouse revealed by correlating callosal and striate-extrastriate connections. Vis Neurosci. 3(1):59–69.
Paxinos G, Franklin KBJ. 2003. The mouse brain in stereotaxic coordinates. 2nd ed.. San Diego (CA): Academic Press.
Reiner A, Veenman CL, Medina L, Jiao Y, Del MN, Honig MG. 2000. Pathway tracing using biotinylated dextran amines. J Neurosci Methods. 103(1):23–37.
Rockland KS, Ojima H. 2003. Multisensory convergence in calcarine visual areas in macaque monkey. Int J Psychophysiol. 50(1–2):19–26.

Roger M, Arnault P. 1989. Anatomical study of the connections of the primary auditory area in the rat. J Comp Neurol. 287(3):339–356.
Romanski LM, LeDoux JE. 1993. Organization of rodent auditory cortex: anterograde transport of PHA-L from MGv to temporal neocortex. Cereb Cortex. 3(6):499–514.
Rouiller EM, Simm GM, Villa AE, De Ribaupierre Y, De Ribaupierre F. 1991. Auditory corticocortical interconnections in the cat: evidence for parallel and hierarchical arrangement of the auditory cortical areas. Exp Brain Res. 86(3):483–505.
Ryugo DK, Killackey HP. 1974. Differential telencephalic projections of the medial and ventral divisions of the medial geniculate body of the rat. Brain Res. 82(1):173–177.
Scheel M. 1988. Topographic organization of the auditory thalamocortical system in the albino rat. Anat Embryol. 179(2):181–190.
Schroeder CE, Foxe JJ. 2002. The timing and laminar profile of converging inputs to multisensory areas of the macaque neocortex. Brain Res Cogn Brain Res. 14(1):187–198.
Schroeder CE, Lakatos P, Kajikawa Y, Partan S, Puce A. 2008. Neuronal oscillations and visual amplification of speech. Trends Cogn Sci. 12(3):106–113.
Shi CJ, Cassell MD. 1997. Cortical, thalamic, and amygdaloid projections of rat temporal cortex. J Comp Neurol. 382(2):153–175.
Smiley JF, Falchier A. 2009. Multisensory connections of monkey auditory cerebral cortex. Hear Res. 258(1–2):37–46.
Smith PH, Manning KA, Uhlrich DJ. 2010. Evaluation of inputs to rat primary auditory cortex from the suprageniculate nucleus and extrastriate visual cortex. J Comp Neurol. 518(18):3679–3700.
Stein BE, Meredith MA, Wallace MT. 1993. The visually responsive neuron and beyond: multisensory integration in cat and monkey. Prog Brain Res. 95:79–90.
Stein BE, Wallace MT. 1996. Comparisons of cross-modality integration in midbrain and cortex. Prog Brain Res. 112:289–299.
Stiebler I, Neulist R, Fichtel I, Ehret G. 1997. The auditory cortex of the house mouse: left-right differences, tonotopic organization and quantitative analysis of frequency representation. J Comp Physiol A Sens Neural Behav Physiol. 181(6):559–571.
Stosiek C, Garaschuk O, Holthoff K, Konnerth A. 2003. In vivo two-photon calcium imaging of neuronal networks. Proc Natl Acad Sci U S A. 100(12):7319–7324.
Sumby WH, Pollack I. 1954. Visual contribution to speech intelligibility in noise. J Acoust Soc Am. 26(2):212–215.
Tsiola A, Hamzei-Sichani F, Peterlin Z, Yuste R. 2003. Quantitative morphologic classification of layer 5 neurons from mouse primary visual cortex. J Comp Neurol. 461(4):415–428.
Verbny YI, Erdelyi F, Szabo G, Banks MI. 2006. Properties of a population of GABAergic cells in murine auditory cortex weakly excited by thalamic stimulation. J Neurophysiol. 96(6):3194–3208.
Wagor E, Mangini NJ, Pearlman AL. 1980. Retinotopic organization of striate and extrastriate visual cortex in the mouse. J Comp Neurol. 193(1):187–202.
Wallace MT, Meredith MA, Stein BE. 1998. Multisensory integration in the superior colliculus of the alert cat. J Neurophysiol. 80(2):1006–1010.
Wang Q, Burkhalter A. 2007. Area map of mouse visual cortex. J Comp Neurol. 502(3):339–357.
White EL, Hersch SM. 1982. A quantitative study of thalamocortical and other synapses involving the apical dendrites of corticothalamic projection cells in mouse SmI cortex. J Neurocytol. 11(1):137–157.
Winer JA, Prieto JJ. 2001. Layer V in cat primary auditory cortex (AI): cellular architecture and identification of projection neurons. J Comp Neurol. 434(4):379–412.
Wree A, Zilles K, Schleicher A. 1983. A quantitative approach to cytoarchitectonics. VIII. The areal pattern of the cortex of the albino mouse. Anat Embryol (Berl). 166(3):333–353.
Zilles K, Wree A. 1985. Cortex: areal and laminar structure. In: Paxinos G, editor. The rat nervous system. Sydney (Australia): Academic Press. p. 375–415.